Soft Matter

Universal Localization Transition Accompanying Glass Formation: Insights from Efficient Molecular Dynamics Simulations of Diverse Supercooled Liquids

Journal:	*Soft Matter*
Manuscript ID	SM-ART-10-2018-002051.R1
Article Type:	Paper
Date Submitted by the Author:	01-Dec-2018
Complete List of Authors:	Hung, Jui-Hsiang; University of Akron, Department of Polymer Engineering Patra, Tarak; University of Akron, Department of Polymer Engineering Meenakshisundaram, Venkatesh; University of Akron, Department of Polymer Engineering Mangalara, Jayachandra Hari; University of Akron, Department of Polymer Engineering Simmons, David; University of South Florida, Chemical and Biomedical Engineering

Soft Matter

ARTICLE

Universal Localization Transition Accompanying Glass Formation: Insights from Efficient Molecular Dynamics Simulations of Diverse Supercooled Liquids

Received 00th January 20xx,
Accepted 00th January 20xx

DOI: 10.1039/x0xx00000x

www.rsc.org/

Jui-Hsiang Hung[a], Tarak K. Patra[a], Venkatesh Meenakshisundaram[a], Jayachandra Hari Mangalara[a], and David S. Simmons*[b]

The origin of the precipitous dynamic arrest known as the glass transition is a grand open question of soft condensed matter physics. It has long been suspected that this transition is driven by an onset of particle localization and associated emergence of a glassy modulus. However, progress towards an accepted understanding of glass formation has been impeded by an inability to obtain data sufficient in chemical diversity, relaxation timescales, and spatial and temporal resolution to validate or falsify proposed theories its physics. Here we first describe a strategy enabling facile high-throughput simulation of glass-forming liquids to nearly unprecedented relaxation times. We then perform simulations of 51 glass-forming liquids, spanning polymers, small organic molecules, inorganics, and metallic glass-formers, with longest relaxation times exceeding one microsecond. Results identify a universal particle-localization transition accompanying glass formation across all classes of glass-forming liquid. The onset temperature of non-Arrhenius dynamics is found to serve as a normalizing condition leading to a master collapse of localization data. This transition exhibits a non-universal relationship with dynamic arrest, suggesting that the nonuniversality of supercooled liquid dynamics enters via the dependence of relaxation times on local cage scale. These results suggest that a universal particle-localization transition may underpin the glass transition, and they emphasize the potential for recent theoretical developments connecting relaxation to localization and emergent elasticity to finally explain the origin of this phenomenon. More broadly, the capacity for high-throughput prediction of glass formation behavior may open the door to computational inverse design of glass-forming materials.

Introduction

Materials ranging from polymers to metals commonly develop solid-like character in the absence of pronounced structural ordering via a process known as glass formation.[1–3] This transition is characterized by a smooth 16-order increase in relaxation time and viscosity on cooling towards the glass transition temperature T_g.[4] The search for a fundamental understanding of the rich spectrum of temperature-dependent paths[5] by which dynamic arrest occurs through the glass transition is a grand challenge of materials science and condensed matter physics.[6]

A major hypothesis for the origin of this transition posits that dynamical arrest is driven by an onset of particle localization, and associated emergence of a glassy modulus, at low temperatures and high frequencies. This localization takes the form of an emergence of a transient 'cage' prior to the onset of particle diffusion, within which particles' trajectories become increasingly compact on cooling. This long-anticipated connection between relaxation and localization provides a core concept underlying multiple theories of the glass transition, including Mode Coupling Theory[7], elastic activation theories[8], free volume theory[4], and the Elastically Collective Nonlinear Langevin Equation theory[9]. Perhaps the simplest intuitive arguments for such a relationship connect the free energy barrier for structural relaxation to the length scale of localization.[4,8–13] However, this connection has not led to a generally accepted fundamental understanding of glass formation, for two reasons. First, and most fundamentally, the onset of localization has not itself been shown to be universal. Therefore, relationships between relaxation and localization potentially relate two non-universal phenomena rather than identify an underlying universal transition.

More broadly, robust confirmation of *any* theory of the glass transition has been prevented by a foundational challenge: experiments generally lack access to sufficient spatial and temporal resolutions to definitively resolve the nature of the glass transition, while in most cases : *"simulations … cannot access the deeply supercooled regime since they probe only down to of order the dynamical crossover temperature"*[14], at a "crossover relaxation time" τ_c in the range of 10^3 to 10^6 ps.[9,14–18] Beyond this point, "It is possible that other physics dominates…"[16], such that structure/property relations and theoretical frameworks based on data at time scales less than τ_c

[a] Department of Polymer of Engineering, University of Akron, 250 South Forge St., Akron, OH 44325, United States
[b] Department of Chemical and Biomedical Engineering, University of South Florida, Tampa, Florida, 33612, United States

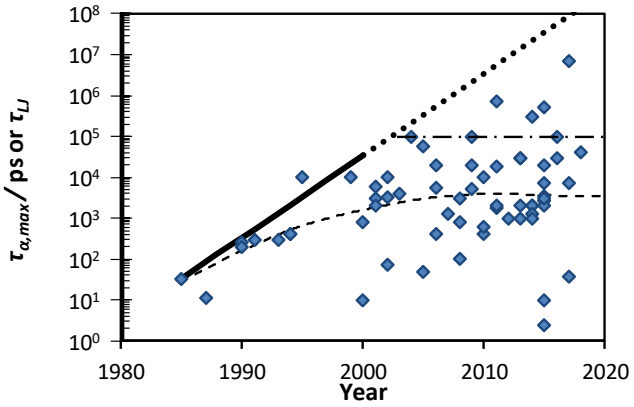

Figure 1. Maximum directly observed, in-equilibrium, mean segmental relaxation times τ_α reported in a representative sample of published molecular dynamics simulations studies performed on commercially available hardware as a function of year (blue diamonds)[12,20–80]. The solid black line is the Moore's law behavior of maximum τ_α realized from 1985 to 2000. The dotted line is the extrapolated Moore's law behavior for 2000 to 2015. The dashed line is a spline fit to the entire data set, illustrating that the average maximum relaxation time has plateaued since approximately 2005. The dot-dashed line is the upper-limit timescale of most simulations, in the range of 10^5 ps.)‡

may fail in the deeply supercooled regime that is more relevant to applications of glass-forming materials.

A molecular-simulation approach to establishing theoretical understanding of the glass transition must therefore incorporate data including relaxation times approaching and preferably exceeding 10^6 ps. Moreover, if these simulations are to establish physics that are universal to glass-forming liquids rather than specific to a particular model system, they should span diverse chemistries and classes of glass-former. However, a survey of published molecular dynamics simulations over the last 30 years[12,19–79] indicates that, with few exceptions, the longest system-mean in-equilibrium-relaxation-times τ_α probed by most molecular dynamics simulations studies have been less than 10^5 ps, with a typical value in the range of $10^3 – 10^4$ ps (see Figure 1)‡. This reflects a more than decade-old breakdown of expected Moore's law improvements in typical simulated in-equilibrium relaxation times, with simulations first reaching a timescale of 10^5 ps by the year 2005. Even had the Moore's law growth of the pre-2000 era continued, simulation times approaching the 100-second timescale of the experimental glass transition would not be expected until the year 2048. Given the current stagnation of these simulated times, it is not clear that the experimental-timescale glass transition will ever be directly probed by molecular simulation, barring some qualitative change in the nature of computing hardware such as viable commercial-scale quantum computers. In the immediate term, however, a more urgent fundamental goal is facile access to timescales approaching and exceeding the crossover timescale noted above, in the range of nanoseconds to microseconds.

Beyond the problem of establishing a fundamental understanding of the glass transition, the generally slow pace of these simulations – a high quality simulation of glass formation can require weeks on significant computing equipment – prevents the use of these simulations for high-throughput simulation of a broad range of glass-forming materials. This type of throughput is needed both to ensure that mechanist insights are universal to all glass-forming liquids and to enable computationally-driven design of glassy materials. Even at a coarse-grained level, glass formation depends on a large matrix of molecular properties. In polymers, for example, it is influenced by molecular weight, backbone stiffness, size and stiffness of side-groups or side-chains, and intermolecular interactions[80,81]. Establishing structure/property relations that enable design of polymers with targeted glass formation behaviour will require simulations spanning thousands of combinations of these molecular properties, demanding use of widely available commercial computer architectures. This type of computationally-driven design has been targeted as a key goal of modern materials science[82], such that this presents a major barrier to the advance of these materials.

Here, we describe a simulation strategy providing a ~100 fold improvement in the efficiency of typical simulations probing the in-equilibrium dynamics of supercooled liquids. First, we begin by briefly describing current standard strategies for simulation of the glass transition and supercooled liquid dynamics. For further discussion of many aspects of the simulation of glass-forming liquids, we refer the reader to a recent review by Baschnagel et al.[83] We describe our new strategy, called Predictive Stepwise Quenching (PreSQ), for simulation of the glass transition. Third, we show that it enables both facile access to the deeply supercooled regime and high-throughput simulation of supercooled liquid dynamics.

By employing this strategy to simulate glass-formation in an unprecedented set of 51-glass formers, spanning metals, polymer, small-organic molecules, and inorganic glass-formers, we establish a new set of simulation data suitable to the identification of universal physics of the glass transition. We employ this dataset to identify a universal localization transition accompanying glass formation and probe its relationship to dynamic arrest.

Strategies and challenges in simulations of the glass transition

We begin with a brief review of standard strategies for simulation of the glass transition. When the goal is simply to determine a glass transition temperature T_g, simulations commonly employ a linear temperature quench inspired by calorimetric experiments[17,84,85]. The glass transition is then determined based on the temperature at which the temperature dependence of the system's energy or volume undergoes a change in slope from liquid to glassy values. The primary factor recommending this method is its simplicity – it is straightforward to implement and can be easily understood by analogy to calorimetry and dilatometry experiments. However, it has multiple shortcomings. Because of the large quench rates involved in simulation, it yields values of T_g that are far removed from those of experiment, with no robust method of correcting for this offset. Linear quenches also tend to vastly over-equilibrate the material at high temperatures, where relaxation is rapid, and this method is therefore computationally inefficient. Furthermore, this method is not aimed at obtaining

in-equilibrium dynamics at temperatures above T_g but rather at determining T_g itself via a non-equilibrium quench simulation. In many practical cases, it is of great importance to predict the temperature dependence of dynamics in the glass-forming liquid and not simply T_g itself. Examples range from prediction of processing characteristics to study of ion conductivity in next-generation battery materials[86–88]. Moreover, the question of the temperature dependence of dynamics is more deeply implicated in the question of fundamental physics of the glass transition than is the value of T_g itself. For these reasons, this method is poorly suited to the study of the supercooled liquid state.

A more suitable approach for this problem employs an initial quench to obtain configurations over a range of (typically evenly spaced) temperatures, and then subjects each of these configurations to an isothermal annealing step to achieve a well-defined equilibrium state. This naturally lends itself to obtaining in-equilibrium data over a range of temperatures in the supercooled state. By allowing for reduced annealing times at high temperature where relaxation is rapid, this method provides a more efficient approach to the glass transition. Because annealing at different temperatures is completely parallelizable, this strategy also makes better use of modern computer hardware. For these reasons, this is the state-of-the-art approach to modern simulation study of the supercooled state dynamics and the glass transition.

Despite this success, the 15-year plateau in most relaxation times achieved in simulations (figure 1) can be largely attributed to two unresolved challenges of simulation in the deeply supercooled state. These problems originate from the fact that the temperature dependence of segmental relaxation time upon approach to the glass transition is super-Arrhenius in the majority of glass-forming liquids[17,85] and is generally unknown at the outset of simulation. This presents a bootstrapping problem: prior knowledge of this temperature dependence is needed to efficiently select optimal temperatures and equilibration times to observe the targeted timescale of dynamics in equilibrium, yet the temperature dependence of τ_α is precisely the property one seeks to predict upon simulation of glass formation in a new material.

The first issue concerns the problem of temperature selection: if one wishes to observe an in-equilibrium segmental relaxation time of, say, 1 μs, it is necessary to choose the temperature at which the system exhibits that relaxation time. However, this temperature is not known at the outset of simulation. Because of the super-Arrhenius nature of dynamics in the supercooled state, at lower temperatures the relaxation time becomes highly sensitive to temperature, such that a small error in the target temperature can lead either to a relaxation time that is orders of magnitude short of the target or can move simulations into a relaxation-time range in which an orders-of-magnitude longer relaxation time makes equilibration computationally impossible. For this reason, it is common for simulation studies employing a linearly-spaced temperature quench to report maximum in-equilibrium relaxation times that fall considerably short of targeted values.

Second, the required annealing time to reach equilibrium at a given temperature is generally understood to be roughly proportional to the segmental relaxation time at that temperature. Since, in general, one does not know the temperature dependence of τ_α at the outset of simulating a new system, it is unclear how long one must anneal to reach equilibrium. For this reason, it is very common for simulation studies to both involve excessively long (by up to orders of magnitude) equilibrations at high temperature and to waste time attempting equilibrations at low temperatures at which long relaxation times make equilibrium simulation computationally hopeless.

These problems have two consequences – they make it very difficult to obtain in-equilibrium relaxation time data appreciably beyond 1-10 ns, and they result in a waste of up to 99% of simulation time on either excessive (high temperature) or hopeless (low temperature) equilibration runs. An improved protocol must therefore both facilitate precise targeting of temperatures exhibiting desired maximum relaxation times and enable efficient annealing runs achieving equilibrium configurations with a minimum of waste.

Methods

Quantification of relaxation behaviour

As reflected above, the central challenge in the simulation of glass-forming liquids is the efficient determination of in-equilibrium relaxation time data over a wide range of time scales upon approach to T_g. We therefore begin by describing our approach for quantification of relaxation time data from simulation. At this stage, we assume that one is working with equilibrium configurations; the question of how to obtain these configurations efficiently is addressed in the next subsection.

As in experiment, there are numerous measures of relaxation that can be employed in simulation to quantify the temperature dependence of supercooled liquid dynamics. Moreover, unlike simple liquids, supercooled liquids frequently exhibit decoupling between distinct dynamical processes[89–94], such that no two measures of relaxation rate are guaranteed to exhibit the same temperature dependence in the glass formation range. These decouplings are not fully understood fundamentally and there is no predictive understanding of the extent to which any chosen pair of dynamical processes will be decoupled. The selection of a particular relaxation function is therefore a question of the problem under consideration, or, more commonly, is simply a matter of convention.

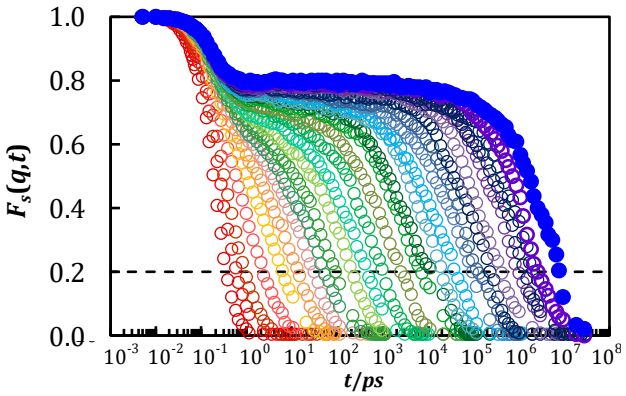

Figure 2. Time evolution of the self-part of intermediate scattering function for the standard attractive bead-spring polymer simulated in this work. Data sets represent increasingly lower temperatures from left to right.

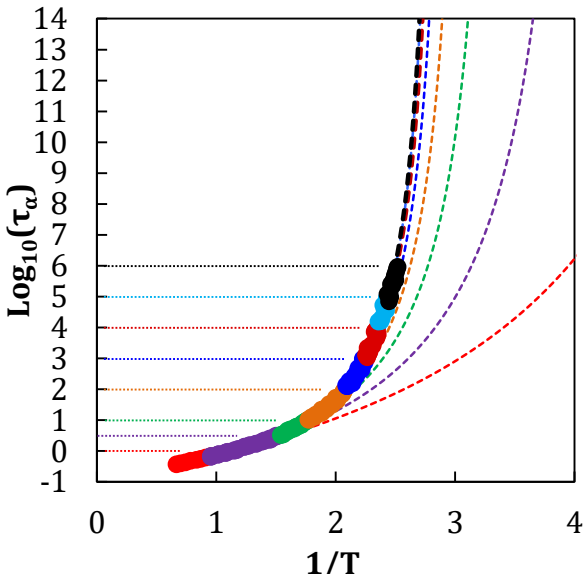

Figure 3. Relaxation time vs inverse temperature data for the bead-spring polymer, illustrating use of the PreSQ algoirhtm to probe increasingly longer relaxation times by descending from high temperature to low temperature regimes defined by τ_α targets. Dotted lines denote the upper τ_α targets in successive τ_α regimes. Dashed lines are the VFT fits to the cumulative equilibrium T's up to the particular regime denoted by the same colour with the τ_α target. Solid circles are in-equilibrium relaxation time data, with colours demoting the regimes where they were collected.

In this discussion, we focus on the self-part of the intermediate scattering function F_s as a commonly employed measure of relaxation in simulation. This relaxation function is essentially equivalent to the relaxation function obtained via time-of-flight incoherent neutron scattering, such that it has a direct relationship to experiment. It is computed as

$$F_s(\mathbf{q},t) = \frac{1}{N}\sum_{j}^{N}\left\langle \exp\left[-i\mathbf{q}\cdot\left(\mathbf{r}_j(t)-\mathbf{r}_j(0)\right)\right]\right\rangle \qquad (1)$$

where $\boldsymbol{q}$ is a wavevector, t is time, $\boldsymbol{r}_j(t)$ is the position of particle j at time t, the summation is over all N particles in the system, and the brackets denote an ensemble average. In order to convert this three dimensional (in $\boldsymbol{q}$-space) relaxation function to a single-dimensional function, it is then typical to sum over values of $\boldsymbol{q}$ of like magnitude to arrive at the function $F_s(q,t)$, where the wavenumber q is the magnitude of the wavevector $\boldsymbol{q}$. In our implementation, this is accomplished by discretizing $\boldsymbol{q}$-space into a grid and then sorting grid points (discretized $\boldsymbol{q}$-vectors) into spherical shells corresponding to a discretized set of wavenumbers. For large q, there can be an extremely large number of wavevectors corresponding to each wavenumber, such that an average over all possible $\boldsymbol{q}$ becomes computationally intractable. When the number of wavenumbers per wavevector exceeds 300, we therefore average over a randomly chosen set of 300 wave-vectors corresponding to that wavenumber to obtain $F_s(q,t)$.

At this point it is necessary to select a particular wavenumber q at which to define a structural relaxation time. Because the dependence of relaxation time on q for this function is not well-characterized as a general matter, this is again a matter of convention. The most common choice is the wavenumber q^* corresponding to the first peak in the structure factor[23,66,93,95–100]. This selection is made by analogy to the full intermediate scattering function, where the de Gennes narrowing phenomenon[101] is commonly expected to lead to a local maximum in relaxation time at this value of q. However, there is no evidence for such a maximum in the self-part of the relaxation function, where the Gaussian approximation suggests that τ_α should scale to leading order as q^{-2}. When comparing differing systems of similar but not identical q^*, we therefore generally prioritize use of a consistent value of q over precise use of a system-dependent q^* in each system when using this relaxation function.

This procedure generally leads to a relaxation function of the form shown in Figure 2. One must now choose some method for extracting a relaxation time from this function. Again, this is a matter of convention. One common approach is to define a relaxation time as the zeroth moment of this distribution function. This is commonly viewed as rigorous, but in fact is merely chosen by analogy to the relationship between the viscosity and the stress relaxation function; there is no formal statistical mechanical basis for viewing the zeroth moment of $F_s(q,t)$ as providing a uniquely correct definition of the relaxation time. This approach also faces issues of numerical convergence that place particularly large computational demands on data collection periods, and can therefore be a somewhat computationally expensive approach. An alternate approach widely used in the literature is to define the relaxation time as the time at which $F_s(q,t)$ relaxes to a fixed value, typically either e^{-1} or 0.2[56,92,95,102]. The latter convention has the advantage that it differs only modestly from the integral method when the relaxation function is described by a stretched exponential with stretching exponents in the range of 0.3 to 1, which is the typical scenario for glass-forming liquids. In this work we therefore adopt this approach as a computationally efficient definition of the alpha relaxation time τ_α. We emphasize that when employing this convention it is essential to spot-check the raw relaxation functions to ensure that they do not possess anomalous low magnitude long-ranged tails or multistep relaxation behaviour that would complicate this approach.

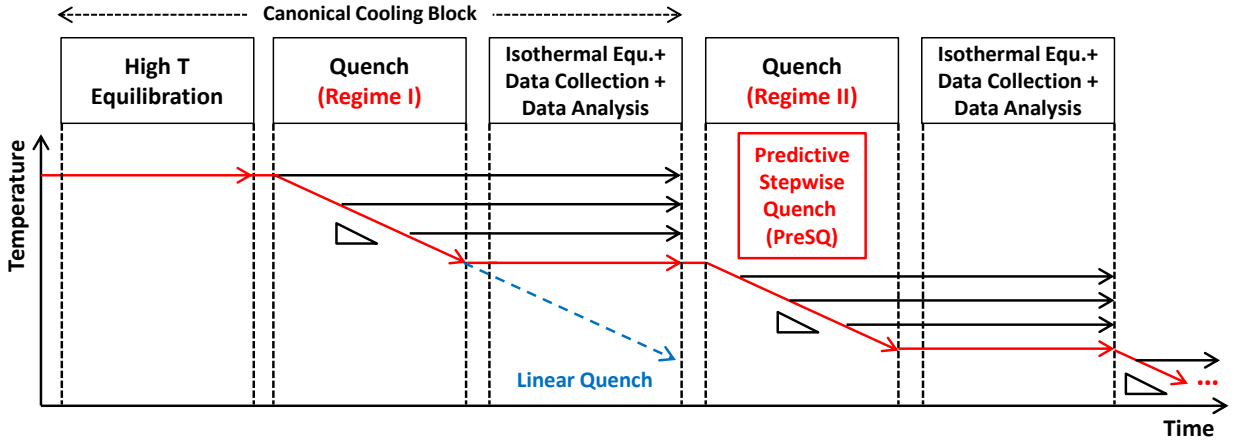

Figure 4. Schematic showing the stepwise quench procedure adopted by PreSQ.

We further emphasize that none of these conventional choices are in any way required by the algorithm described in the next section. Instead, the algorithm and its implementation work equally well with other choices of relaxation function (for example reorientational relaxation functions also commonly used in the literature), other choices of wavenumber, or other conventions for extracting a relaxation time from the relaxation function. We simply focus here on the conventions described above as a reasonable test case.

Predictive Stepwise Quench algorithm

Here we describe a protocol for simulation of dynamics in glass-forming liquids that overcomes the challenges discussed in the introduction to provide efficient access to in-equilibrium supercooled dynamics. This protocol, Predictive Stepwise Quenching (PreSQ), dramatically increases the efficiency of these simulations, allowing facile access to in-equilibrium relaxation times approaching and exceeding one μs on modest computational equipment. In addition to this 2-3 order of magnitude increase in the range of easily accessible in-equilibrium relaxation times, PreSQ yields higher-temperature-resolution data than standard approaches[102–104]. The algorithm is equally amenable to bead-spring, coarse-grained, and all-atom models. Below we describe the results of simulations employing this protocol to probe the supercooled liquid state in model systems at each of these levels of chemical detail.

PreSQ is an iterative quench algorithm that solves the bootstrapping problem associated with the two central challenges to simulation of the supercooled state described above – a priori selection of temperatures corresponding to target relaxation times, and a priori determination of the appropriate equilibration (annealing) time at each temperature. It does this while making maximal use of modern parallel computing architectures to achieve maximal simulation efficiency.

As shown by Figure 3, the essential strategy of PreSQ is to iteratively simulate relaxation at progressively lower temperatures and longer relaxation times, using a continuously-improved extrapolation from higher temperatures to select new simulation temperatures and equilibration times. As shown schematically by Figure 4 in time/temperature space, the algorithm specifically divides relaxation-time space into windows of relaxation time of 1 decade or less in span. It begins by obtaining relaxation times in the shortest-time window, and then iteratively explores longer-time windows, using data from shorter times to select temperatures suitable to each progressively longer relaxation-time window. An example of these relaxation time windows (τ_1=10^0, τ_2=$10^{0.5}$, τ_2=10^1, …, τ_8=10^6ps), is illustrated by the dashed lines in the schematic of Figure 3.

The first step of this algorithm is to obtain relaxation time data in the shortest relaxation time window by brute force. As shown in Figure 4 PreSQ begins by annealing a simulation of the target system into equilibrium at very high temperature. This temperature is chosen to be far above the expected glass transition range of the class of materials under consideration and may exceed typical degradation temperatures of that material class in experiment. For example, for most polymeric materials it is reasonable to begin at a temperature in the range of 1000K. This allows for rapid realization of an equilibrium configuration based on a pre-determined high temperature annealing period (typically 10 ps).

From this point, the protocol is bootstrapped by determining τ_α over a range of very high temperatures for which relaxation is expected to occur within 1 ps. To do so, the high temperature equilibration is subject to a rapid linear temperature quench over a range of temperatures expected to remain far above T_g. For example, in most polymers a quench from 1000K to 800K is reasonable. Configurations are saved at n evenly spaced temperatures over this range, with each then subject to an isothermal annealing period of 10 ps. Relaxation times for these configurations are then quantified during a subsequent data collection run at each temperature via the approach described above.

At this point, the algorithm performs several checks to ensure that each configuration is indeed in equilibrium. First, in-equilibrium supercooled liquids typically exhibit a segmental

relaxation process conforming to a stretched exponential form with stretching exponent less than or equal to one. The algorithm therefore attempts to perform a stretched exponential fit to the alpha relaxation process. Failure of this fit to converge to a high value of the coefficient of determination R^2 is treated as a potential sign of a non-equilibrium state or otherwise anomalous behaviour. Similarly, convergence to a value of the stretching exponent beta significantly greater than one is also treated as a sign of a potentially non-equilibrium state. In either case, the configuration is flagged as potentially non-equilibrium and is not used in future steps of the algorithm.

Next, the algorithm checks the measured relaxation time against the equilibration time. As discussed in the introduction, good equilibration generally requires an equilibration period τ_{eq} of at least a multiple α of the relaxation time τ_α, such that $\tau_{eq} \geq \alpha\tau_\alpha$. As shown below, testing indicates that $\alpha = 1$ is frequently sufficient to yield equilibrium value of the relaxation time. We employ a standard value of $\alpha = 10$ out of an abundance of caution, except where otherwise noted. The algorithm thus performs a check of the above inequality, and in the case that $\tau_{eq} < \alpha\tau_\alpha$, the configuration is flagged as potentially non-equilibrium and is again not used in future algorithm steps as valid dynamical data.

At this point, the algorithm checks the number of in-equilibrium relaxation times surviving the prior checks. If this number is at least half of the number of temperatures targeted in this time window, the algorithm proceeds with the next step. If not, it re-tries this step with a new set of temperatures, with the same number of temperatures as in previous attempts, spaced over a reduced temperature range in an effort to find more in-equilibrium configurations at higher temperature. This check ensures that sufficient in-equilibrium data is obtained over each relaxation time window. In our experience, in well-behaved systems these additional attempts are rare, and a repeated inability to identify equilibrium configurations over the projected temperature range is often a sign of confounding phenomena such as crystallization.

After these checks, the algorithm fits all in-equilibrium relaxation time data obtained thus far to a functional form for the temperature-dependence of local relaxation time. A common such form is the Vogel-Fulcher-Tammann (VFT) relation[105–107]. However, we find that this functional form tends to overpredict relaxation times, and we thus frequently employ an alternate form proposed by Schmidtke et al[108]. In testing, we found that use of the VFT form at high temperature and the Schmidtke form at lower temperatures tends to yield the largest number of 'good' projections of appropriate temperatures for each relaxation time window.

In either case, this fit is then employed to select *n* new temperatures predicted evenly spaced over the next relaxation time window (typically a decade longer). The algorithm then performs a fast temperature quench from the lowest previously simulated in-equilibrium temperature over this new temperature range. Each of these new configurations is then subject to an isothermal equilibration period of α times the new longest targeted τ_α for the new relaxation time window. Relaxation times are then determined at these temperatures based upon subsequent data collection runs. Data are checked for equilibration state, and the overall process is iterated until the ultimate target relaxation time is reached.

Throughout this discussion, we have treated the number of temperatures *n* per relaxation time decade as a variable. This number should generally be selected based upon a combination of the relaxation-time resolution desired and the computational hardware employed. The computing cluster employed in this work consists of compute nodes with 16 CPU cores and 2 GPUs per compute node. We thus target 8 temperatures per time window and typically assign 1 core and 1/8 GPU per temperature, such that each simulated glass-former occupies ½ node. For the longest relaxation times probed, we sometimes instead employ n = 4 to allow an allocation of 2 cores and ¼ GPU to each temperature, facilitating faster simulations in the longest time window.

Molecular dynamics implementation

We employ the PreSQ algorithm to perform simulations of 51 distinct glass-forming liquids, including polymeric, small-molecule organic, inorganic, and metallic glass-formers. Simulations employ standard, well-validated force fields previously published in the literature, including 47 systems simulated at the all-atom level, as described below. Simulated systems include the following: multiple molecular weights of polystyrene (PS), polyisobutylene (PIB), polybutadiene (PB) polyvinylchloride (PVC); a series of poly(n-alkyl acrylates) (PC_nA); polyetherimide (PEI) the standard Kremer-Grest bead-spring glass-former (KG); organic small molecules α-D glucose , glycerol, trehalose, and ortho-terphenyl (OTP); inorganic glass-former SiO_2; a copper/silver binary metallic glass-former; and a binary Lennard-Jones fluid designed to model metallic glass-formers (b-LJ).

The system employed for primary validation of the PreSQ algorithm is a bead-spring polymer employing an attractive extension of the Kremer-Grest model[109] that has been widely employed to study glass formation in polymers[54,56,92,96,102,110–114]. At a bead-model level, we also simulate a Binary Lennard Jones (LJ) model employing a standard binary LJ potential previously employed in the literature[115].

For chemically-realistic polymers and organic molecules, we use the OPLS-AA and OPLA-UA force fields,[116,117] which are

tabulated in the Tinker molecular modeling package,[118,119] except for the case of for polyacrylates. Instead, we used a modified OPLS-AA dihedral potential and partial charges[120] for all-atom polyacrylate simulations, based on evidence that this modification leads to an improved description of alkyl side chain structure and dynamics. All polymers with tacticity are atactic. Coarse-grained simulations of polystyrene employ the previously studied united atom OPLS potential and a "MARTINI" model for PS[121]. Simulations of Cu_4Ag_6 employ the EAM potential with parameters obtained from the NIST Interatomic Potentials Repository[122,123]. Simulations of SiO_2 employ the Morse Potential[124].

For all the all-atom polymers, united-atom polystyrene, small organic molecules reported in this study, the initial molecular structures and the atom type specifications are prepared by *Avogadro*[125], a molecular editing and rendering software. MD simulations are conducted using the LAMMPS open source code [126]. Moltemplate [127] is used to assist in preparing input files for LAMMPS simulation. For other systems simulated in this study, including the bead-spring polymer, Martini polystyrene[121], binary LJ mixture and the metal alloy, initial atom coordinates are generated by PACKMOL [128]. All MD simulations employed the *Verlet* algorithm [129] for time integration. Simulations are conducted in the isothermal-isobaric (NPT) ensemble using the Nose-Hoover thermostat and barostat as implemented in LAMMPS. For systems in LJ units, we use common conversions of one LJ distance unit $\sigma \sim 1$ nm and one LJ time unit $\tau_{LJ} \sim 1$ ps in reporting results.

In general, the rate of MD simulation of atomistic models is limited by the need for a very short (typically 1 fs) integration time step to due to the presence of high-frequency vibrations involving low-mass hydrogen atoms. In order to improve simulation rates in hydrogen-containing atomistically detailed models, masses of all the atoms in a system are commonly adjusted to reduce the hydrogen atoms' average instantaneous velocity while preserving thermodynamic properties and the overall mass of the molecule[130,131]. In order to increase the efficiency of the MD simulations, masses of the hydrogen rich systems are redistributed in this manner this study. Specifically, the mass of hydrogen atoms are increased, and the mass of the heavier atoms (carbon) is decreased to their average mass, keeping the molecular mass unchanged in a standard manner [132]. The redistribution of mass enables us to use an integration time step of 3 fs for all all-atom polymers and small-molecule organics. We note that this naturally impacts dynamics, particularly at high frequency. However, in testing we found that the impact on glass-formation behaviour was relatively weak, likely as a consequence of the central role for interparticle interactions and caging effects, rather than short-time ballistic motion, in supercooled relaxation dynamics.

During the course of the extremely long simulations performed at the lowest temperatures considered in this study, preliminary simulations indicated that residual center-of-mass momentum tends to build up due to the random perturbations from the thermostatting. In the Kremer-Grest polymers, the momentum accumulation effect on the resulting relaxation time does not become significant until after τ_α is longer than 10^4 τ_{LJ}. In order to eliminate any momentum accumulation effect, all simulations in this study have performed momentum zeroing for every 1-10 ps by subtracting the residual center-of-mass velocity from all constituent atoms. The same procedure is done for the angular momentum to ensure the system is free from linear and angular momentum bioldup. In order to verify that this procedure does not have any impact on measured dynamics beyond the prevention of aphysical momentum buildup, we performed preliminary simulations of the Kremer-Grest model verifying that relaxation times were not dependent on the use of a momentum fix for temperatures at which no momentum buildup was present.

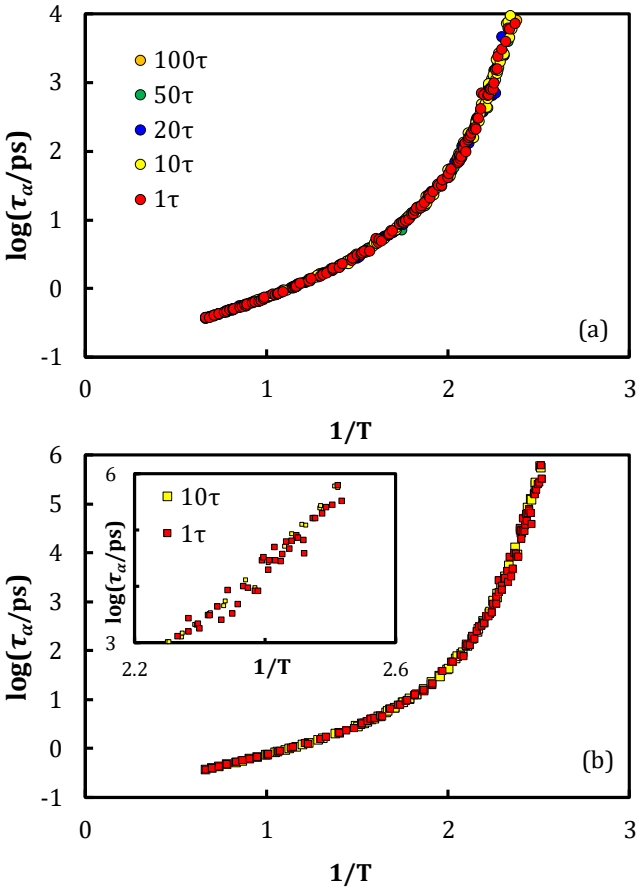

Figure 5. Simulated τ_α vs T data for a 1600-bead (a) and 8000-bead (b) systems. Each data set is generated with a target equilibration period of α times τ_α at each temperature (as described in the text), with the factor α given by the legends. Inset of part b focuses on the longest time scales simulated.

Results

Validation of equilibration protocol and reproducibility

As described above, this protocol employs an equilibration criterion requiring that equilibration at each temperature be of duration of 10 τ_α. We therefore first verify that a factor of 10 is sufficient. To do so, we perform simulations of the KG polymer using alternate equilibration-time criteria of 1, 5, 50, and 100 times τ_α. As shown in Figure 5a, equilibration times in the range of 5 to 100 τ_α have no effect on segmental relaxation time, indicating that segmental relaxation has reached its equilibrium

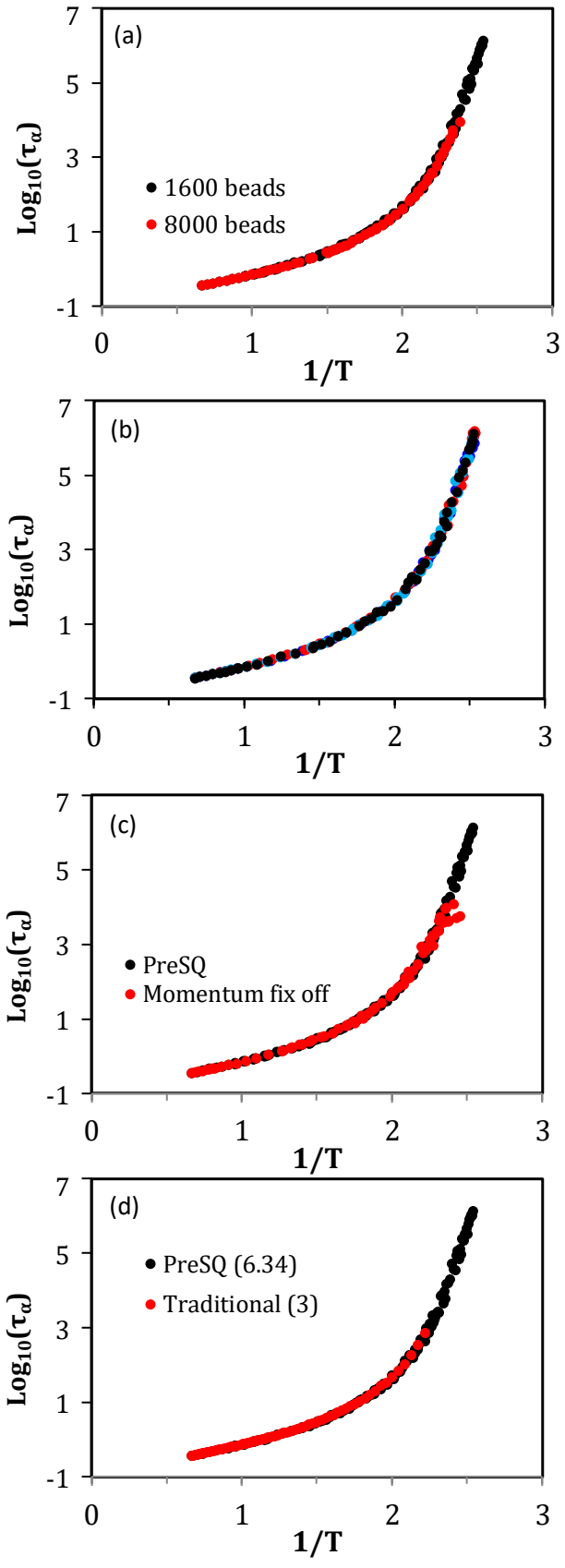

Figure 6. Relaxation time vs inverse temperature for (a) two system sizes, (b) four trials, (c) runs with momentum-zeroing turned on and off, and (d) PreSQ vs standard simulation approach for the bead spring polymer.

rate in this range. We additionally perform this test for a larger system with 8000 beads, and we again find no systematic differences between relaxation time data after an equilibration of 1 vs 10 times τ_α (Figure 5b). These results indicate that an equilibration period of 1 τ_α is sufficient to obtain equilibrium segmental relaxation times. Throughout the simulations reported here, we employ an equilibration period of 10 τ_α out of an abundance of caution, except for the Kremer-Grest bead spring polymer in the relaxation time range $10^6 < \tau_\alpha < 10^7$, where we employ an equilibration period of 2 τ_α to allow access to longer time scales. Moreover, a comparison of results for the 1600-bead and 8000-bead simulations Figure 6a indicate that this system size range is above the threshold below which finite size effects on relaxation time become pronounced.

To verify the reproducibility of the data produced by this protocol, we compare relaxation time data from 4 independent simulation runs handled by the same protocol. As shown by Figure 6b segmental relaxation time data from these 4 simulations exhibit no systematic deviations and minimal noise.

As noted in the methods section, we employ a protocol wherein center of mass momentum is infrequently set to zero to prevent a momentum buildup. As shown by Figure 6c, at time scales for which momentum buildup is absent, this protocol does not alter the relaxation dynamics of the system, validating this approach.

Comparison to standard methods

The details of equilibration protocols employed by distinct groups in the literature differ considerably, and it is thus not possible to report in a general manner the efficiency improvement of this method. As a reasonable estimate, we compare performance for a PreSQ simulation of the bead-spring polymer to our previously published simulation[102] of the same system using standard quench-and-anneal methods described in the introduction, as implemented previously by our group. The previously published simulation probed dynamics in a Kremer-Grest polymer melt up to a maximum in-equilibrium relaxation time of 10^3. That simulation used a standard quench and anneal protocol and simulated a total of 1.6×10^7 LJ time units, integrated across all temperatures. A PreSQ simulation of the same system by the protocol above required simulation of 1.9×10^5 LJ time units up to a comparable time scale, an O(100) fold decrease in simulation time requirements. As shown by Figure 6d, the two methods yield equivalent relaxation time results up to the time scale easily accessible to the standard approach. Of this approximate 100x speedup, approximately 10-fold is a consequence of employing isothermal equilibrations of duration 10 times rather than 100 times τ_α. This factor is likely to be fairly non-universal due to the large range of equilibration time conventions employed in the literature. The other ~10x speedup is a consequence of a more judicious selection of temperatures and equilibration periods to better track with τ_α, avoiding over-equilibration and wasted efforts at equilibrating inaccessible temperatures.

The key component of this comparison is the efficiency improvement associated with automated selection of equilibration times tracking with the growing relaxation time on

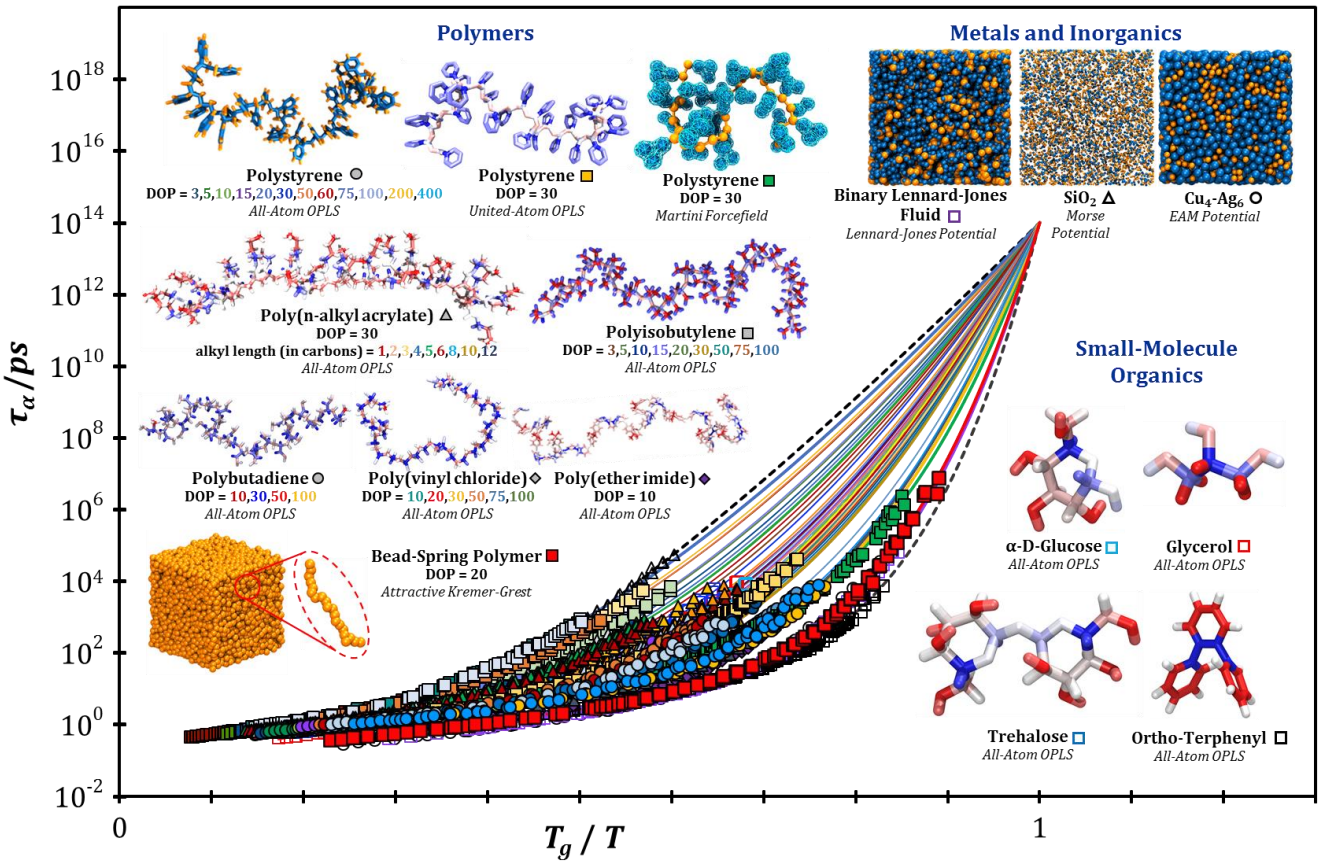

Figure 7. Angell plot[5] of simulated segmental relaxation times illustrating wide range of relaxation-time temperature dependences for systems considered in this study. Lines are fits to the cooperative model of Schmidtke et al.[109] Insets are renderings, made in VMD[134] of the simulated glass-forming materials included in this plot with corresponding symbols. Numbers next to "DOP" for polymers list degrees of polymerization simulated, with the text colour indicating the symbol colour employed for that DOP.

cooling. The 10-fold improvement reported above in this respect likely represents a lower-bound improvement since we have focused this comparison on a system simulated to only 10^3 time units. Simulations to longer times, such as the simulation to a relaxation time of 10^6, reported below, encounter dramatically larger challenges with temperature and equilibration time selection as a consequence of the increasingly strong temperature dependence of dynamics at low temperatures. This is likely the reason that there have been few simulations of segmental relaxation dynamics in this range – efforts to do so have generally involved very computationally expensive brute force efforts to equilibrate over a range of lower temperature, or time-intensive efforts to manually infer required relaxation times from higher-temperature data.

Indeed, as shown by Figure 2, relaxation time data for the bead-spring polymer simulated to long times via the PreSQ algorithm exhibit a well-developed plateau spanning approximately 4 decades in time – a feature of deeply supercooled liquids that is rarely if ever observed in simulation. As shown in Figure 7, the corresponding segmental relaxation time approaches 10^7 – the longest in-equilibrium mean segmental relaxation time ever reported for this system.

In addition to allowing facile access to long-times, this algorithm facilitates efficient high-throughput simulation of the glass transition. For example, many physically informative simulations of the glass transition over the last 10 years have probed maximum τ_α values on the order of 1 ns. At a bead-spring level, this algorithm enables access to this timescale in approximately 2.5 hours, such that over 500 bead-spring glass formers can be simulated to this time-scale per month on a single node. At the AA level, simulation to this timescale requires approximately 4 days on half of a high performance computing node.[5] Below we combine these two advances – facile access to long times and to high throughput simulations or diverse chemistries – to obtain data spanning a broad range of time scales and glass-forming liquid chemistries.

Relaxation data

Relaxation times obtained for the 51 polymeric, small-molecule organic, inorganic, and metallic glass-formers simulated in this study include over 3000 relaxation time data points, with longest in-equilibrium segmental relaxation times near 10 μs, spanning a total simulated time of approximately 3 ms and reflecting approximately 7 x 10^5 GPU-accelerated computing core hours. As shown by an "Angell plot"[5] of these systems' segmental relaxation time τ_α vs T_g-normalized temperature[108] (Figure 7)[133], they exhibit a large range of deviations from Arrhenius relaxation behaviour (i.e. a large range of fragilities of glass formation), comparing favourably to the diversity seen in experiments.[5] The resulting simulations provide the required

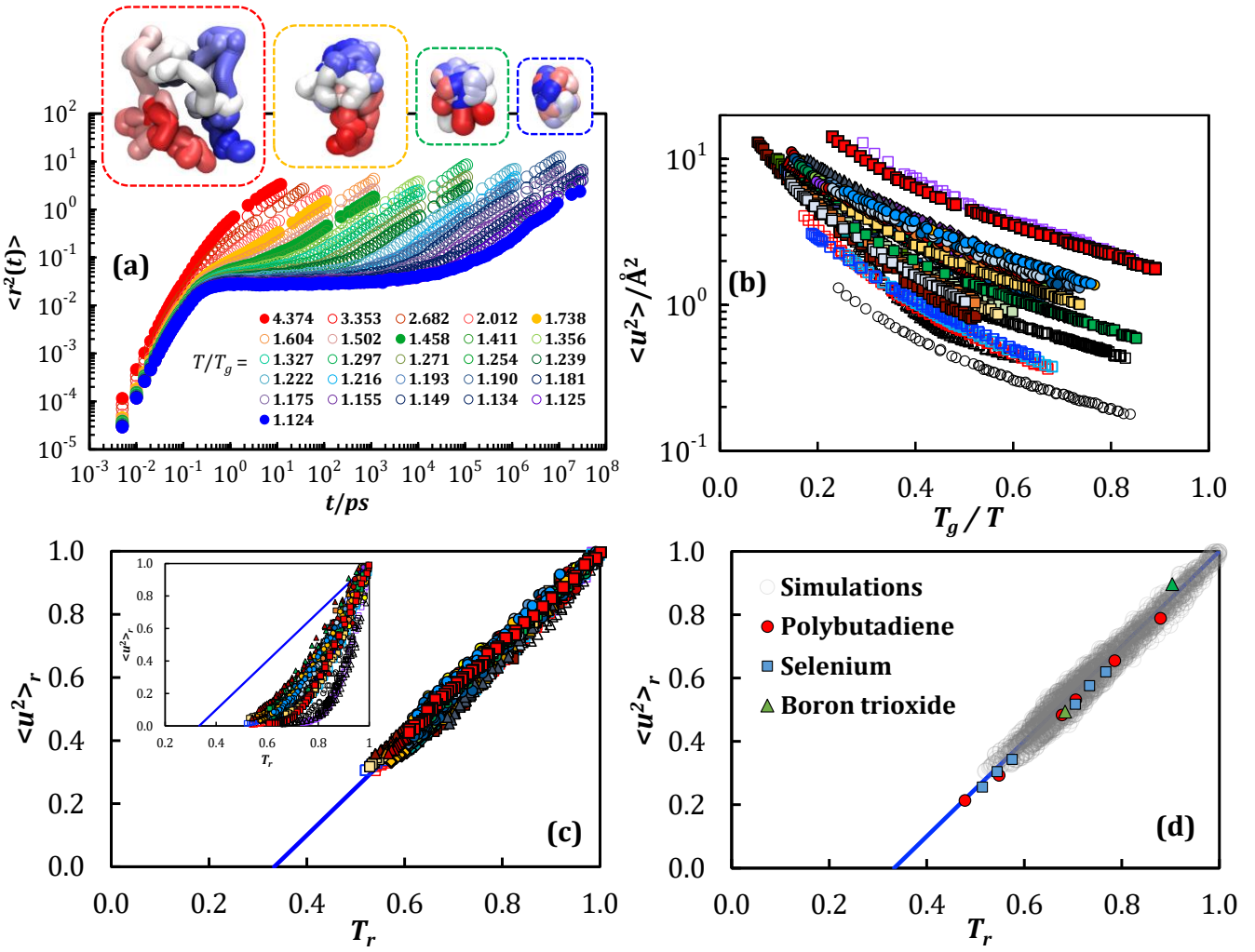

Figure 8. (a) Mean square displacement from simulation of a bead-spring polymer model, illustrating emergence of particle localization. The insets illustrate the onset of localized (caged) dynamics, with each inset showing a typical trajectory of the centre 1/6 of a particle over 10 ps, at a temperature denoted by the outline colour and the legend. (b) Plot of simulated $<u^2>$ vs T_g/T for all systems in this study, reflecting the reduction in the localization length scale on cooling. (c) Collapse of $<u^2>_r$ vs T_r at temperatures below T_A for all systems simulated in this study to equation (2) in the text, corresponding to the blue line. Inset shows the same plot but with $<u^2>$ determined at a fixed time of 100 ps rather than at the cage onset time employed in the main figure and described in the text. (d) The same plot as (c), but including several published experimental sets of $<u^2>$ data between 1 and 10 ps as determined from time of flight neutron scattering experiments.

temporal and spatial resolutions across diverse systems to identify universal physics of the glass transition.

Universal localization transition during glass formation

We begin by asking whether the onset of particle localization during glass formation is universal in nature. As shown by Figure 8a, localization takes the form of a transient regime of dynamics in which atoms, molecules, or polymer segments rattle within a cage of their neighbours. The size of this cage is quantified in simulation[12,98,134] and experiment[135–138] by the Debye-Waller factor $<u^2>$, which is the mean square displacement at the onset of this caging regime. Here we define $<u^2>$ uniformly, at approximate cage onset times of $10^{-0.15}$ ps in chemically realistic polymers and $10^{-0.55}$ ps otherwise, in order to eliminate the time of measurement as an implicit adjustable parameter. These time windows are selected to minimize contamination by segmental relaxation to the extent possible over the entire glass formation range and enable determination of $<u^2>$ at relatively high temperatures. Localization becomes more severe as the system progresses towards T_g, as manifested in Figure 8b for the systems simulated here by a continuous contraction of the localization size scale $<u^2>$.

To establish universal features of this transition we employ as a normalizing condition the onset temperature of glass formation T_A, [66,139] defined as the temperature below which the relaxation time first deviates from an Arrhenius temperature dependence (i.e. the first point of deviation from the high-temperature linear regime in Figure 7). [81] The onset temperature T_A is specifically determined for each system via the following procedure. We first fit data at high temperature, where relaxation exhibits an Arrhenius temperature dependence, to the Arrhenius form $\tau_\alpha = \tau_\infty \exp(E_A/kT)$. We then define T_A as the temperature at which the quantity $kT\ln(\tau_\alpha/\tau_\infty)/E_A = 1.15$, with a penalized cubic spline employed for smoothing and interpolation, signifying a 15% deviation of the relaxation process from the extrapolation of its high-temperature Arrhenius behavior. We define τ_A and $<u^2>_A$ as the values of τ_α

Table 1. For simulated systems, degree of polymerization, onset temperature T_A, and log(relaxation time) and Debye-Waller factor at T_A .

Material	DOP	T_A	$\log(\tau/ps)_{TA}$	$\langle u^2 \rangle$ at T_A
AA PIB	3	328 K	0.729	2.15 Å^2
AA PIB	5	458 K	0.632	2.46 Å^2
AA PIB	10	556 K	0.758	2.35 Å^2
AA PIB	15	675 K	0.537	2.87 Å^2
AA PIB	20	680 K	0.615	2.72 Å^2
AA PIB	30	716 K	0.610	2.72 Å^2
AA PIB	50	741 K	0.587	2.75 Å^2
AA PIB	75	743 K	0.616	2.64 Å^2
AA PIB	100	701 K	0.758	2.42 Å^2
AA PS	3	507 K	0.525	2.71 Å^2
AA PS	5	601 K	0.543	2.83 Å^2
AA PS	10	698 K	0.559	2.99 Å^2
AA PS	15	765 K	0.517	3.17 Å^2
AA PS	20	750 K	0.655	2.90 Å^2
AA PS	30	782 K	0.609	3.03 Å^2
AA PS	50	760 K	0.730	2.80 Å^2
AA PS	60	789 K	0.674	2.93 Å^2
AA PS	75	816 K	0.622	3.04 Å^2
AA PS	100	783 K	0.687	2.94 Å^2
AA PS	200	808 K	0.689	2.94 Å^2
AA PS	400	803 K	0.703	2.90 Å^2
AA PVC	10	562 K	0.524	2.34 Å^2
AA PVC	20	651 K	0.445	2.55 Å^2
AA PVC	30	676 K	0.445	2.57 Å^2
AA PVC	50	671 K	0.503	2.43 Å^2
AA PVC	75	709 K	0.438	2.58 Å^2
AA PVC	100	690 K	0.483	2.47 Å^2
AA PEI	10	918 K	0.569	2.80 Å^2
AA PB	10	486 K	0.706	2.67 Å^2
AA PB	30	581 K	0.752	2.71 Å^2
AA PB	50	539 K	0.478	3.17 Å^2
AA PB	100	666 K	0.546	3.14 Å^2
AA PC_1A	30	757 K	0.436	3.70 Å^2
AA PC_2A	30	670 K	0.542	3.49 Å^2
AA PC_3A	30	614 K	0.630	3.25 Å^2
AA PC_4A	30	614 K	0.575	3.38 Å^2
AA PC_5A	30	618 K	0.537	3.50 Å^2
AA PC_6A	30	633 K	0.466	3.64 Å^2
AA PC_8A	30	512 K	0.890	2.60 Å^2
AA $PC_{10}A$	30	537 K	0.740	2.79 Å^2
AA $PC_{12}A$	30	545 K	0.689	2.85 Å^2
UA-PS	30	520 K	1.25	1.91 Å^2
Martini-PS	30	532 K	1.21	1.37 Å^2
AA Glycerol	NA	475 K	0.438	1.19 Å^2
AA α-D-Glucose	NA	585 K	0.868	0.884 Å^2
AA Trehalose	NA	839 K	0.301	1.43 Å^2
AA OTP	NA	346 K	1.27	0.654 Å^2
AA Cu_4Ag_6	NA	876 K	0.560	0.353 Å^2
AA SiO_2	NA	2553 K	1.32	0.839 Å^2
KG	20	0.633	0.582	0.0413 σ^2
b-LJ	NA	0.467	1.03	0.0350 σ^2

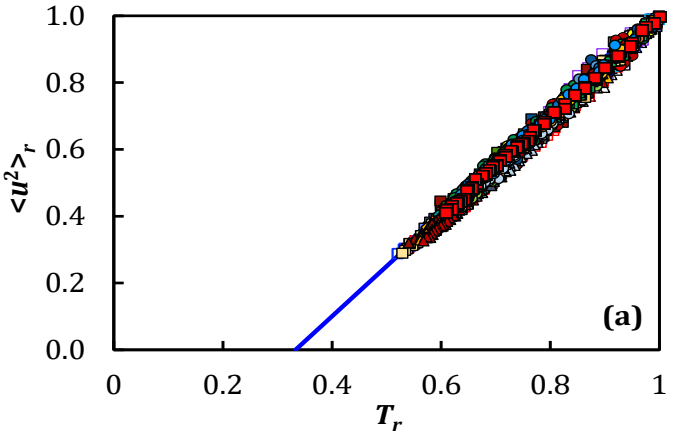

Figure 9. Collapse of $\langle u^2 \rangle_r$ vs T_r at temperatures below T_A for all systems simulated in this study to equation (2) in the text, with slight system-by-system adjustments to the caging time.

and $\langle u^2 \rangle$ at this temperature, using a penalized cubic spline of each quantity for data smoothing and interpolation. This procedure is fully automated and admits no researcher adjustment of results from system to system. Table 1 provides a list of resulting T_A, τ_α, and $\langle u^2 \rangle_A$ values obtained via this procedure for all systems simulated here.

As shown by Figure 8c, plotting a reduced Debye-Waller factor $\langle u^2 \rangle_r = \langle u^2 \rangle / \langle u^2 \rangle_A$ vs reduced temperature $T_r = T/T_A$ for the more than 2000 data points simulated at temperatures below T_A reveals a universal zero-parameter collapse to the form

$$\langle u^2 \rangle_r = (3T_r - 1)/2 \qquad (2)$$

This collapse is also shown on a system-by-system basis in the SI to permit distinct visualization of each chemistry simulated. The sole system exhibiting visual evidence of curvature is SiO_2, and this is likely due to the extreme difficulty of determining T_A accurately in this highly Arrhenius system; our determination of T_A is entirely automated, and we do not implement any strategy to improve the definition described above for use in highly Arrhenius systems. The linearity of this form is consistent with recent findings of Leporini and coworkers.[140] However, the introduction of renormalization by the onset condition of glass formation leads to an apparently universal, zero-parameter collapse of $\langle u^2 \rangle$ vs temperature data. Since T_A is determined based upon deviation from Arrheniusness in τ_α data rather than based on any fit to $\langle u^2 \rangle$, this collapse is in no way a forced fit. The collapse can be further improved with slight system-by-system adjustments to this caging time (see Figure 9). Evidently, these results identify a quantitatively universal localization transition below the onset temperature T_A, with an extrapolated approach to complete localization at a temperature $T_0 = T_A/3$.

The finding that normalization by the onset condition provides a universal zero-parameter collapse of the localization scale identifies T_A as a deeply significant condition in the physics of glass formation. This interpretation is amplified by earlier work, which has identified T_A as corresponding to an onset of caged dynamics[4], dynamic heterogeneity, cooperative molecular or

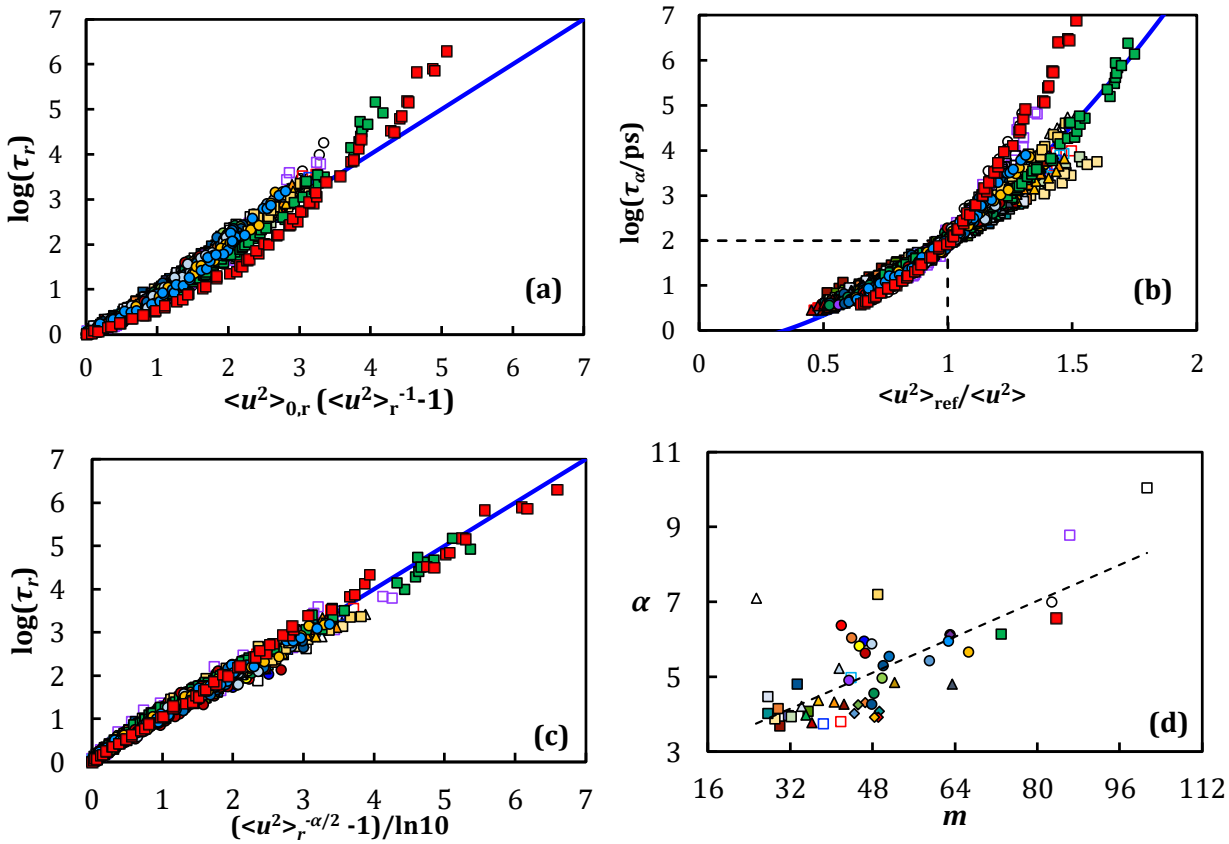

Figure 10. (a) Test of equation (3) in the text. (b) Test of equation (5) in the text, with a reference timescale of 10^2 ps. (c) Test of equation (8) in the text, with fit parameters α shown in part (d).

segmental motion[2,81,97], and phonon delocalization[141]. Normalization by T_A has also been shown to lead to corresponding states behaviour of relaxation times in a set of metallic glass formers[142], and T_A has been argued to correlate with the fragility of glass formation.

Why has this universality gone unnoticed in experiments studying the temperature dependence of $\langle u^2 \rangle$? The majority of experiments have focused on values of $\langle u^2 \rangle$ determined via quasi-elastic neutron scattering (QENS), typically at energies corresponding to times of order 30 ns. To test the effect of determining $\langle u^2 \rangle$ at these longer time scales, in Figure 8c inset we attempt to recreate the collapse to equation (2) with $\langle u^2 \rangle$ data collected at a fixed time of 100 ps. As shown by this figure, the temperature dependence of $\langle u^2 \rangle$ becomes nonlinear (as typically reported by 30 ns QENS) and nonuniversal at this time scale, a result of contamination by the segmental relaxation process. While it is possible to obtain O(ps) $\langle u^2 \rangle$ data through time of flight neutron scattering, only a small fraction of studies have employed this methodology due to its relative difficulty. When this is done, the resulting <u2> data is typically linear in temperature, as shown in recent work.[140]

Experimental confirmation of the universality identified above thus requires data meeting two challenging requirements. First, $\langle u^2 \rangle$ data must be obtained on the order of 1-10 ps or less in order to avoid pronounced contamination by the segmental relaxation process[135,143]. Second, T_A must be directly accessible without the intervention of chemical degradation at the very high temperatures commonly involved. In order to test equation (2) against experiment, we have identified three systems for which data meeting these criteria are available in the literature: boron trioxide[144,145], selenium[146], and polybutadiene[147,148].

We use several methods to estimate T_A for the experimental systems. For B_2O_3, we employ the method described above for simulations, but we apply it to published high resolution experimental viscosity data[145]. Based on the approximate 10 ps timescale of T_A described in a section below, for polybutadiene we determine T_A based on a slight extrapolation of high temperature τ_α data[148] to a 10 ps timescale. T_A for selenium is determined in the same manner using published viscosity data, employing a common conversion wherein a viscosity of 1 Pa·s is approximately equated a relaxation time of 10^{-10} s for non-polymeric liquids. These approaches yield values of T_A of 804 K for boron trioxide, 626 K for selenium, and 432 K for polybutadiene.

As shown by Figure 8d, these data also collapse to equation (2) without adjustable parameters, supporting the proposition that this form describes a localization transition universally characterizing glass formation in all materials. Given connections between $\langle u^2 \rangle$ and free volume [4,149], this universal collapse may underpin a linear relationship between T_g and fractional free volume at T_g observed across numerous experimental polymeric glass formers. [150]

Together, these results suggest a need for an expanded focus on understanding the nature of the onset of non-Arrheniusness in glass-forming liquids. Unlike posited critical-like temperatures below the glass transition temperature, T_A is experimentally accessible with fairly standard methods in a substantial range of glass-formers (although it tends to be prohibited in many polymers due to the onset of chemical degradation at temperatures well above T_g). Study of this onset condition therefore affords the potential to obtain new insights into glass formation without resort to heroic strategies needed to access relaxation behaviour at sub-T_g temperatures[151,152].

Relationship between relaxation and localization

Does this universal localization transition drive the growth in relaxation time upon approach to T_g seen in Figure 7? As discussed above, a large number of theoretical frameworks have posited such a connection. As an initial test of this proposition within this new set of cohesive data, here we probe the predictions of two related theoretical frameworks connecting slowing relaxation dynamics to the onset of particle localization.[4,8,10,11] First, classical elastic activation models suggest that the activation energy of relaxation and the magnitude of localized molecular motions $\langle u^2 \rangle$ are both controlled by the same effective localizing potential[8]. It follows that the quantity $k_BT/\langle u^2 \rangle$, where k_B is Boltzmann's constant, reports on the value of the effective spring constant of this potential and the barrier height to escape the cage.[8] The canonical formalization of this scenario, pioneered by Hall and Wolynes, leads to a simple exponential relationship between τ and $1/\langle u^2 \rangle$. When written in terms of a reduced relaxation time $\tau_r = \tau/\tau|_{TA}$ in a manner consistent with equation (2) and compelled to agree with the observed relaxation behaviour at T_A, this relation can be expressed with a single free parameter:

$$\tau_r = \exp\left[\frac{u_0^2}{\langle u^2 \rangle_A}\left(\frac{1}{\langle u^2 \rangle_r} - 1\right)\right] \qquad (3)$$

where u_0 is interpreted with the Hall-Wolynes model as an escape distance. As shown by Figure 10a, the data exhibit considerable systematic deviation from this functional form, consistent with prior work.[12]

Larini et al. proposed a zero parameter extension of this functional form based upon introduction of a Gaussian distribution for the 'escape distance' u_0:[12]

$$\log \tau_\alpha = A + B\frac{\langle u^2 \rangle_g}{\langle u^2 \rangle} + C\left(\frac{\langle u^2 \rangle_g}{\langle u^2 \rangle}\right)^2 \qquad (4)$$

where the values of A, B, and C were argued to be universal for all glass-forming liquids once $\langle u^2 \rangle$ is normalized by its value $\langle u^2 \rangle_g$ at the experimental timescale glass transition.[12] To test this proposal at computationally-accessible timescales, we employ an equivalent form of equation (4) in which a normalizing reference $\langle u^2 \rangle_r$ is defined at an arbitrary timescale τ_{ref} while remaining mathematically consistent with the original functional form[153]:

$$\log \tau_\alpha = A + BX_r\frac{\langle u^2 \rangle_{ref}}{\langle u^2 \rangle} + CX_r^2\left(\frac{\langle u^2 \rangle_{ref}}{\langle u^2 \rangle}\right)^2, \qquad (5)$$

where X_r is a renormalizing factor given self-consistently by

$$X_r = \langle u^2 \rangle_g / \langle u^2 \rangle_{ref} = \left(-B + \sqrt{B^2 - 4AC + 4C\log\tau_{ref}}\right)\Big/2C\,. \quad (6)$$

As shown by Figure 10b, our data do not exhibit a collapse to this form. We emphasize that finding this does not exclude the possibility of a relationship between τ_α and $\langle u^2 \rangle$ of the general form of equation 4; however, it is inconsistent with the proposition[12] that this relationship obtains at a zero-parameter level.

We now test an alternate approach based upon free volume theory. Free volume theories argue that the barrier to relaxation is inversely related to the available space for particle motion v_f, [11,13] which within an isotropic model of localization is given by $v_f \propto \langle u^2 \rangle^{3/2}$.[134] Both the harmonic localization perspective and the free volume approach thus lead to an equation of the form [4]

$$\tau = \tau_0 \exp\left[\left(u_0^2/\langle u^2 \rangle\right)^{\alpha/2}\right], \qquad (7)$$

where $\alpha = 2$ under the assumption of harmonic localization or 3 for isotropic free volume theory. As noted above, $\alpha = 2$ does not lead to a good collapse of the data, even with a single adjustable parameter.

We have previously generalized this form to account for the observed local anisotropy[4] and anharmonicity[154] of localization in supercooled liquids by noting that these deviations from ideality can be described by a system-dependent value of α, with larger values corresponding to more anisotropic and/or anharmonic localization. In prior work, we have demonstrated that introduction of caging anisotropy to a free volume model of glass formation leads to equation (7), with values of α greater than 3 corresponding to an increasing temperature dependence of localization anisotropy[4].

Using the ansatz $u_0^2 \approx \langle u^2 \rangle_A$ [4,66] and defining a reduced relaxation time as $\tau_r = \tau_\alpha / \tau_\alpha|_{T=T_A}$, we arrive at a scaling model for the effect of localization on relaxation in the presence of caging anisotropy and anharmonicity:

$$\ln \tau_r = \langle u^2 \rangle_r^{-\alpha/2} - 1\,. \qquad (8)$$

As shown by Figure 10c, equation (8) indeed describes the relationship between relaxation and localization, using only the single parameter α, with values shown in Figure 10d, that is expected to be greater than 3 by this scaling model in the case of anistropic caging. The fit values of α are between 3 and 6 for most of the systems simulated, which is qualitatively reasonable within the expectations of the scaling theory (Figure 10d). However, there are several systems with excursions to higher values of α, and we emphasize that the form of this relationship is strongly sensitive to α.

These results thus emphasize that the relationship between relaxation and localization is likely non-universal, with at least one-material dependent parameter involved in this relationship. Equation (8) provides a semi-empirical scaling relationship between these quantities; this type of approach has previously been used to predict relaxational behaviour at temperatures where this would normally be inaccessible to simulation[155]. Although this relationship is evidently system-dependent, because the underlying localization transition is evidently universal, this transition must be considered a primary candidate for the mechanism of glassy dynamic arrest. More broadly, recent years have seen the development of a much more robust, force level theory linking relaxation to localization, the Elastically Cooperative Nonlinear Langevin Equation theory of supercooled liquid dynamics[9,156,157]. This theory also predicts a *qualitatively* universal relationship between localization and relaxation that *quantitatively* varies based upon material-dependent quantities. The present results therefore lends new weight to support to the promise of this approach.

From a practical standpoint, given that we find that both equations (2) and (8) empirically describe glass formation, we can now combine them to arrive at an expression relating temperature and relaxation time:

$$3T_r = 2\left(\ln \tau_r + 1\right)^{-2/\alpha} + 1. \qquad (9)$$

Here α can be obtained from the fit of equation (8) to τ_α vs $<u^2>$ data. As shown by Figure 11, equation (9) indeed predicts the relationship between temperature and relaxation time for all of the systems within this study.

We note that it is possible to reframe equation (9) in a form similar to the Vogel-Fulcher-Tammann (VFT) equation[158,159]:

$$\tau = \tau_A \exp(-1)\exp\left[\left(\frac{2T_0}{T - T_0}\right)^{\alpha/2}\right], \qquad (10)$$

where $T_0 = T_A/3$ for all glass formers. As in the VFT expression, T_0 is an extrapolated (and not necessarily real) divergence temperature. Unlike in the VFT expression, this temperature has a universal value when normalized by the onset temperature T_A.

Conclusions

The PreSQ algorithm for simulation of supercooled liquid dynamics enables efficient simulation of glass-forming liquids to long times and across diverse chemistries by solving the bootstrapping problem of temperature and equilibration time selection. While the algorithm is presently implemented with pure molecular dynamics, it is in principle further extensible via the use of accelerated annealing strategies. At present, the standard protocol involves total simulation time (equilibration plus data collection) of ~20 times the relaxation time at each temperature. Use of rapid annealing strategies could in principle reduce this by a factor of 20 (to a single relaxation time

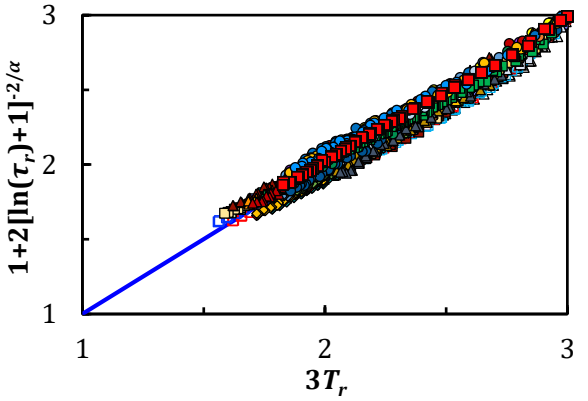

Figure 11. Collapse of τ_α vs T data at temperatures below T_A for all systems simulated in this study to equation (9) in the text.

period) by enabling rapid equilibration is systems large enough to accumulate good statistics with a shorter observation period.

Looking forward, this algorithm removes one of the central impediments to realizing Moore's law scaling of simulated in-equilibrium relaxation times – the bootstrapping problem of temperature and equilibration time selection. The main workaround to this problem in the past has simply been repeated simulation of the same model by the same group over many years, allowing iterative 'in-house' determination of optimal temperatures and times for simulation. This approach, in addition to limiting access to relaxation time scales, also made extension of these simulations into diverse chemistries or model modifications unwieldy and relatively rare. By eliminating this material-specific learning curve, the PreSQ algorithm thus enables facile and high-throughput simulations of a much more diverse set of glass-formers, with implications for both physical understanding and computational design.

We employ this algorithm to simulate relaxation in an unprecedented set of glass-forming liquids, spanning metals, polymers, small-molecules organics, and inorganics. Results point to several key conclusions regarding the nature of the glass transition. First, the onset of localization, accompanying glass formation, is apparently quantitatively universal when subject to normalization by the onset condition of non-Arrhenius dynamics. This finding emphasizes the central physical importance of this onset condition and provides a qualitatively new indicator that particle localization may underlie glassy dynamic arrest at a fundamental level. Second, the relationship between relaxation and localization is nonuniform, such that at least one additional material-dependent quantity is required to capture chemical differences between systems. Indeed, since $<u^2>$ itself behaves in a quantitatively universal manner, it appears that the non-uniformity of its relationship with τ may in fact be the origin of the non-universal spectrum of dynamic arrest pathways (i.e. fragilities) observed in diverse glass-formers.

Theoretical predictions relating relaxation behaviour to the localization scale via the recently developed Elastically Cooperative Nonlinear Langevin Theory of dynamics in the

presence of particle localization[9,156,157] have the potential to further explicate this scenario. Most recently, Phan and Schweizer have shown that this theory predicts only weak system to system variation in the temperature dependence of a mean particle displacement corresponding to the maximum in the effective force resulting from the localizing potential, when both the displacement and the temperature are normalized by their values at the onset. At the same time, this theory predicts strong variation in the temperature dependence of the activation barrier for relaxation from system-to-system[160]. At a high level, this nonuniversality of relaxation behaviour emerges from relatively universal localization behaviour within that theory via the involvement of a naturally chemistry-dependent segmental jump length scale. The present findings appear to be in strong accord which this prediction of the ECNLE theory. Use of the present approach to further quantitatively validate or falsify central propositions of this and other theories of the glass transition should be a central goal of ongoing work in this area.

Conflicts of interest

There are no conflicts to declare.

Acknowledgements

This work was made possible by generous support from the W. M. Keck Foundation. This material is based in part on work supported by the National Science Foundation NSF Career Award grant number DMR1554920. The authors thank C. Martin for computational hardware support, A. Frischknecht for suggesting an improved simulation forcefield for polyacrylates, and A. Dobrynin, M. Cicerone, and K. Schweizer for helpful discussion and editorial advice.

Supplementary information

Electronic supplementary information, including supplementary data. Simulation trajectories will be made available upon request to the corresponding author.

Notes and references

1. Debenedetti, P. G. & Stillinger, F. H. Supercooled liquids and the glass transition. *Nature* **410**, 259–267 (2001).

2. Cavagna, A. Supercooled liquids for pedestrians. *Phys. Rep.-Rev. Sect. Phys. Lett.* **476**, 51–124 (2009).

3. Ediger, M. D. & Harrowell, P. Perspective: Supercooled liquids and glasses. *J. Chem. Phys.* **137**, 080901-080901–15 (2012).

4. Simmons, D. S., Cicerone, M. T., Zhong, Q., Tyagi, M. & Douglas, J. F. Generalized localization model of relaxation in glass-forming liquids. *Soft Matter* **8**, 11455–11461 (2012).

5. Angell, C. A. Formation of Glasses from Liquids and Biopolymers. *Science* **267**, 1924–1935 (1995).

6. Kivelson, S. A. & Tarjus, G. In search of a theory of supercooled liquids. *Nat. Mater.* **7**, 831–833 (2008).

7. Götze, W. *Complex Dynamics of Glass-Forming Liquids : A Mode-Coupling Theory: A Mode-Coupling Theory*. (Oxford University Press, 2008).

8. Dyre, J. C. Colloquium: The glass transition and elastic models of glass-forming liquids. *Rev. Mod. Phys.* **78**, 953–972 (2006).

9. Mirigian, S. & Schweizer, K. S. Elastically cooperative activated barrier hopping theory of relaxation in viscous fluids. I. General formulation and application to hard sphere fluids. *J. Chem. Phys.* **140**, 194506 (2014).

10. Hall, R. W. & Wolynes, P. G. The aperiodic crystal picture and free-energy barriers in glasses. *J. Chem. Phys.* **86**, 2943–2948 (1987).

11. Doolittle, A. K. Studies in Newtonian Flow. II. The Dependence of the Viscosity of Liquids on Free-Space. *J. Appl. Phys.* **22**, 1471–1475 (1951).

12. Larini, L., Ottochian, A., De Michele, C. & Leporini, D. Universal scaling between structural relaxation and vibrational dynamics in glass-forming liquids and polymers. *Nat. Phys.* **4**, 42–45 (2008).

13. White, R. P. & Lipson, J. E. Polymer Free Volume and Its Connection to the Glass Transition. *Macromolecules* **49**, 3987–4007 (2016).

14. Mirigian, S. & Schweizer, K. S. Communication: Slow relaxation, spatial mobility gradients, and vitrification in confined films. *J. Chem. Phys.* **141**, 161103 (2014).

15. Starr, F. W., Douglas, J. F. & Sastry, S. The relationship of dynamical heterogeneity to the Adam-Gibbs and random first-order transition theories of glass formation. *J. Chem. Phys.* **138**, 12A541-12A541-18 (2013).

16. Ediger, M. D. & Harrowell, P. Perspective: Supercooled liquids and glasses. *J. Chem. Phys.* **137**, 080901 (2012).

17. Cavagna, A. Supercooled liquids for pedestrians. *Phys. Rep.-Rev. Sect. Phys. Lett.* **476**, 51–124 (2009).

18. Dudowicz, J., Freed, K. F. & Douglas, J. F. Generalized Entropy Theory of Polymer Glass Formation. in *Advances in Chemical Physics* **137**, 125–222 (Wiley, 2008).

19. Ullo, J. J. & Yip, S. Dynamical Transition in a Dense Fluid Approaching Structural Arrest. *Phys. Rev. Lett.* **54**, 1509–1512 (1985).

20. Anderson, J., Ullo, J. J. & Yip, S. Molecular dynamics simulation of dielectric properties of water. *J. Chem. Phys.* **87**, 1726 (1987).

21. Barrat, J.-L., Roux, J.-N. & Hansen, J.-P. Diffusion, viscosity and structural slowing down in soft sphere alloys near the kinetic glass transition. *Chem. Phys.* **149**, 197–208 (1990).

22. Kob, W. & Andersen, H. C. Testing mode-coupling theory for a supercooled binary Lennard-Jones mixture I: The van Hove correlation function. *Phys. Rev. E* **51**, 4626–4641 (1995).

23. Starr, F. W., Sciortino, F. & Stanley, H. E. Dynamics of simulated water under pressure. *Phys. Rev. E* **60**, 6757–6768 (1999).

24. Aichele, M. & Baschnagel, J. Glassy dynamics of simulated polymer melts: Coherent scattering and van Hove correlation functions. *Eur. Phys. J. E* **5**, 229–243 (2001).

25. Horbach, J. & Kob, W. Relaxation dynamics of a viscous silica melt: The intermediate scattering functions. *Phys. Rev. E* **64**, 041503 (2001).

26. Lewis, L. J. & Wahnström, G. Rotational dynamics in ortho-terphenyl: a microscopic view. *J. Non-Cryst. Solids* **172–174**, **Part 1**, 69–76 (1994).

27. Lewis, L. J. & Wahnström, G. Relaxation of a molecular glass at intermediate times. *Solid State Commun.* **86**, 295–299 (1993).

28. Signorini, G. F., Barrat, J.-L. & Klein, M. L. Structural relaxation and dynamical correlations in a molten state near the liquid–glass transition: A molecular dynamics study. *J. Chem. Phys.* **92**, 1294–1303 (1990).

29. Hiwatari, Y. *et al.* Study of the α and β relaxations in a supercooled fluid via molecular-dynamics simulations. *Phys. Stat. Mech. Its Appl.* **204**, 306–327 (1994).

30. Mossa, S., Di Leonardo, R., Ruocco, G. & Sampoli, M. Molecular dynamics simulation of the fragile glass-former orthoterphenyl: A flexible molecule model. *Phys. Rev. E* **62**, 612–630 (2000).

31. Witt, R., Sturz, L., Dölle, A. & Müller-Plathe, F. Molecular Dynamics of Benzene in Neat Liquid and a Solution Containing Polystyrene. 13C Nuclear Magnetic Relaxation and Molecular Dynamics Simulation Results. *J. Phys. Chem. A* **104**, 5716–5725 (2000).

32. Starr, F. W., Schrøder, T. B. & Glotzer, S. C. Effects of a nanoscopic filler on the structure and dynamics of a simulated polymer melt and the relationship to ultrathin films. *Phys. Rev. E* **64**, 021802 (2001).

33. Colmenero, J., Alvarez, F. & Arbe, A. Self-motion and the alpha relaxation in a simulated glass-forming polymer: Crossover from Gaussian to non-Gaussian dynamic behavior. *Phys. Rev. E* **65**, (2002).

34. Smith, G. D., Borodin, O. & Paul, W. A molecular-dynamics simulation study of dielectric relaxation in a 1,4-polybutadiene melt. *J. Chem. Phys.* **117**, 10350–10359 (2002).

35. F Varnik, J. B. Reduction of the glass transition temperature in polymer films: a molecular-dynamics study. *Phys. Rev. E Stat. Nonlin. Soft Matter Phys.* **65**, 021507 (2002).

36. Lacevic, N., Starr, F. W., Schroder, T. B. & Glotzer, S. C. Spatially heterogeneous dynamics investigated via a time-dependent four-point density correlation function. *J. Chem. Phys.* **119**, 7372–7387 (2003).

37. Smith, G. D., Bedrov, D. & Paul, W. A molecular dynamics simulation study of the α-relaxation in a 1,4-polybutadiene melt as probed by the coherent dynamic structure factor. *J. Chem. Phys.* **121**, 4961–4967 (2004).

38. Tsolou, G., Mavrantzas, V. G. & Theodorou, D. N. Detailed Atomistic Molecular Dynamics Simulation of cis-1,4-Poly(butadiene). *Macromolecules* **38**, 1478–1492 (2005).

39. Baljon, A. R. C., Van Weert, M. H. M., DeGraaff, R. B. & Khare, R. Glass Transition Behavior of Polymer Films of Nanoscopic Dimensions. *Macromolecules* **38**, 2391–2399 (2005).

40. Riggleman, R. A., Yoshimoto, K., Douglas, J. F. & de Pablo, J. J. Influence of Confinement on the Fragility of Antiplasticized and Pure Polymers. *Phys Rev Lett* **97**, 0455021–0455024 (2006).

41. Peter, S., Meyer, H. & Baschnagel, J. Thickness-dependent reduction of the glass-transition temperature in thin polymer films with a free surface. *J. Polym. Sci. Part B-Polym. Phys.* **44**, 2951–2967 (2006).

42. Lombardo, T. G., Debenedetti, P. G. & Stillinger, F. H. Computational probes of molecular motion in the Lewis-Wahnström model for ortho-terphenyl. *J. Chem. Phys.* **125**, 174507 (2006).

43. Zhang, L. & Greenfield, M. L. Relaxation time, diffusion, and viscosity analysis of model asphalt systems using molecular simulation. *J. Chem. Phys.* **127**, 194502 (2007).

44. Tsolou, G., Harmandaris, V. A. & Mavrantzas, V. G. Molecular dynamics simulation of temperature and pressure effects on the intermediate length scale dynamics and zero shear rate viscosity of cis-1,4-polybutadiene: Rouse mode analysis and dynamic structure factor spectra. *J. Non-Newton. Fluid Mech.* **152**, 184–194 (2008).

45. Maragakis, P. *et al.* Microsecond Molecular Dynamics Simulation Shows Effect of Slow Loop Dynamics on Backbone Amide Order Parameters of Proteins. *J. Phys. Chem. B* **112**, 6155–6158 (2008).

46. Chong, S.-H. & Kob, W. Coupling and Decoupling between Translational and Rotational Dynamics in a Supercooled Molecular Liquid. *Phys. Rev. Lett.* **102**, 025702 (2009).

47. Karmakar, S., Dasgupta, C. & Sastry, S. Growing length and time scales in glass-forming liquids. *Proc Nat Acad Sci* **106**, 3675–3679 (2009).

48. Tanis, I. & Karatasos, K. Local Dynamics and Hydrogen Bonding in Hyperbranched Aliphatic Polyesters. *Macromolecules* **42**, 9581–9591 (2009).

49. Terada, Y. & Tokuyama, M. Spatial dimensionality dependence of long-time diffusion on two- and three-dimensional systems near glass transition. *Intermetallics* **18**, 1834–1836 (2010).

50. Kim, K. & Saito, S. Role of the Lifetime of Dynamical Heterogeneity in the Frequency-Dependent Stokes–Einstein Relation of Supercooled Liquids. *J. Phys. Soc. Jpn.* **79**, 093601 (2010).

51. Boland, E. K., Liu, J. & Maranas, J. K. A molecular picture of motion in polyolefins. *J. Chem. Phys.* **132**, 144901 (2010).

52. Puosi, F. & Leporini, D. Universal elastic and plastic effects in the particle caging of polymers and glassforming liquids. *arXiv:1108.4629* (2011).

53. Shi, Z., Debenedetti, P. G., Stillinger, F. H. & Ginart, P. Structure, dynamics, and thermodynamics of a family of potentials with tunable softness. *J. Chem. Phys.* **135**, 084513 (2011).

54. Starr, F. W. & Douglas, J. F. Modifying Fragility and Collective Motion in Polymer Melts with Nanoparticles. *Phys. Rev. Lett.* **106**, 115702 (2011).

55. Harmandaris, V. A., Floudas, G. & Kremer, K. Temperature and Pressure Dependence of Polystyrene Dynamics through Molecular Dynamics Simulations and Experiments. *Macromolecules* **44**, 393–402 (2010).

56. Paul Z. Hanakata, Jack F. Douglas & Francis W. Starr. Local Variation of Fragility and Glass Transition Temperature of Ultra-thin Supported Polymer Films. *J. Chem. Phys.* **137**, 244901 (2012).

57. Fotiadou, S. *et al.* Structure and Dynamics of Hyperbranched Polymer/Layered Silicate Nanocomposites. *Macromolecules* **46**, 2842–2855 (2013).

58. Sengupta, S., Karmakar, S., Dasgupta, C. & Sastry, S. Breakdown of the Stokes-Einstein relation in two, three, and four dimensions. *J. Chem. Phys.* **138**, 12A548 (2013).

59. Puosi, F., De Michele, C. & Leporini, D. Scaling between relaxation, transport and caged dynamics in a binary mixture on a per-component basis. *J. Chem. Phys.* **138**, 12A532-12A532-9 (2013).

60. Hanakata, P. Z., Douglas, J. F. & Starr, F. W. Interfacial mobility scale determines the scale of collective motion and relaxation rate in polymer films. *Nat. Commun.* **5**, 4163 (2014).

61. Klameth, F., Henritzi, P. & Vogel, M. Static and dynamic length scales in supercooled liquids: Insights from molecular dynamics simulations of water and tri-propylene oxide. *J. Chem. Phys.* **140**, 144501 (2014).

62. Xie, S.-J., Qian, H.-J. & Lu, Z.-Y. Polymer brushes: A controllable system with adjustable glass transition temperature of fragile glass formers. *J. Chem. Phys.* **140**, 044901 (2014).

63. Zhang, Z. *et al.* Atomistic Structure of Bottlebrush Polymers: Simulations and Neutron Scattering Studies. *Macromolecules* **47**, 5808–5814 (2014).

64. Rissanou, A. N. & Harmandaris, V. Dynamics of various polymer–graphene interfacial systems through atomistic molecular dynamics simulations. *Soft Matter* **10**, 2876 (2014).

65. Xia, W., Hsu, D. D. & Keten, S. Molecular Weight Effects on the Glass Transition and Confinement Behavior of Polymer Thin Films. *Macromol. Rapid Commun.* **36**, 1422–1427 (2015).

66. Betancourt, B. A. P., Hanakata, P. Z., Starr, F. W. & Douglas, J. F. Quantitative relations between cooperative motion, emergent elasticity, and free volume in model glass-forming polymer materials. *Proc. Natl. Acad. Sci.* **112**, 2966–2971 (2015).

67. Frey, S. *et al.* Simulated glass-forming polymer melts: Dynamic scattering functions, chain length effects, and mode-coupling theory analysis. *Eur. Phys. J. E* **38**, 1–18 (2015).

68. Chakrabarty, S., Karmakar, S. & Dasgupta, C. Dynamics of Glass Forming Liquids with Randomly Pinned Particles. *Sci. Rep.* **5**, 12577 (2015).

69. Wu, R., Qiu, X., Zhang, T., Fu, K. & Yang, X. Atomistic Molecular Insight into the Time Dependence of Polymer Glass Transition. *J. Phys. Chem. B* **119**, 9959–9969 (2015).

70. Davris, T. & Lyulin, A. V. A coarse-grained molecular dynamics study of segmental structure and mobility in capped crosslinked copolymer films. *J. Chem. Phys.* **143**, 074906 (2015).

71. Xu, W.-S., Duan, X., Sun, Z.-Y. & An, L.-J. Glass formation in a mixture of hard disks and hard ellipses. *J. Chem. Phys.* **142**, 224506 (2015).

72. Jaiswal, A., Egami, T. & Zhang, Y. Atomic-scale dynamics of a model glass-forming metallic liquid: Dynamical crossover, dynamical decoupling, and dynamical clustering. *Phys. Rev. B* **91**, 134204 (2015).

73. Ramos, J., Vega, J. F. & Martínez-Salazar, J. Molecular Dynamics Simulations for the Description of Experimental Molecular Conformation, Melt Dynamics, and Phase Transitions in Polyethylene. *Macromolecules* **48**, 5016–5027 (2015).

74. Arbe, A. *et al.* Role of Dynamic Asymmetry on the Collective Dynamics of Comblike Polymers: Insights from Neutron Spin-Echo Experiments and Coarse-Grained Molecular Dynamics Simulations. *Macromolecules* **49**, 4989–5000 (2016).

75. Ninarello, A., Berthier, L. & Coslovich, D. Models and Algorithms for the Next Generation of Glass Transition Studies. *Phys. Rev. X* **7**, 021039 (2017).

76. Sethuraman, V. & Ganesan, V. On the relationship between the local segmental dynamics and the tagged monomer dynamics in lamellar phases of diblock copolymers. *J. Chem. Phys.* **147**, 104901 (2017).

77. Pazmiño Betancourt, B. A., Starr, F. W. & Douglas, J. F. String-like collective motion in the α- and β-relaxation of a coarse-grained polymer melt. *J. Chem. Phys.* **148**, 104508 (2018).

78. Xu, W.-S., Douglas, J. F. & Freed, K. F. Influence of Pressure on Glass Formation in a Simulated Polymer Melt. *Macromolecules* **50**, (2017).

79. Guillaud, E., Merabia, S., Ligny, D. de & Joly, L. Decoupling of viscosity and relaxation processes in supercooled water: a molecular dynamics study with the TIP4P/2005f model. *Phys. Chem. Chem. Phys.* **19**, 2124–2130 (2017).

80. Huang, D. & McKenna, G. B. New insights into the fragility dilemma in liquids. *J. Chem. Phys.* **114**, 5621–5630 (2001).

81. Dudowicz, J., Freed, K. F. & Douglas, J. F. Generalized Entropy Theory of Polymer Glass Formation. in *Advances in Chemical Physics* **137**, 125–222 (Wiley, 2008).

82. Curtarolo, S. *et al.* The high-throughput highway to computational materials design. *Nat. Mater.* **12**, 191–201 (2013).

83. Baschnagel, J. *et al.* Glass transition and relaxation behavior of supercooled polymer melts: An introduction to modeling approaches by molecular dynamics simulations and to comparisons with mode-coupling theory. in *Polymer Glasses* 55–105 (Taylor & Francis, 2016). doi:10.1201/9781315305158-5

84. Barrat, J.-L., Baschnagel, J. & Lyulin, A. Molecular dynamics simulations of glassy polymers. *Soft Matter* **6**, 3430 (2010).

85. Debenedetti, P. G. & Stillinger, F. H. Supercooled liquids and the glass transition. *Nature* **410**, 259–267 (2001).

86. Hoarfrost, M. L. & Segalman, R. A. Conductivity Scaling Relationships for Nanostructured Block Copolymer/Ionic Liquid Membranes. *ACS Macro Lett.* **1**, 937–943 (2012).

87. Choi, U. H. *et al.* Molecular Volume Effects on the Dynamics of Polymerized Ionic Liquids and their Monomers. *Electrochimica Acta* **175**, 55–61 (2015).

88. Choi, U. H. *et al.* Dielectric and Viscoelastic Responses of Imidazolium-Based Ionomers with Different Counterions and Side Chain Lengths. *Macromolecules* **47**, 777–790 (2014).

89. Kumar, S. K., Szamel, G. & Douglas, J. F. Nature of the breakdown in the Stokes-Einstein relationship in a hard sphere fluid. *J. Chem. Phys.* **124**, 214501 (2006).

90. Schweizer, K. S. & Saltzman, E. J. Activated Hopping, Barrier Fluctuations, and Heterogeneity in Glassy Suspensions and Liquids. *J. Phys. Chem. B* **108**, 19729–19741 (2004).

91. Cicerone, M. T., Wagner, P. A. & Ediger, M. D. Translational Diffusion on Heterogenous Lattices: A Model for Dynamics in Glass Forming Materials. *J Phys Chem B* **101**, 8727–8734 (1997).

92. Hung, J.-H., Mangalara, J. H. & Simmons, D. S. Heterogeneous Rouse Model Predicts Polymer Chain Translational Normal Mode Decoupling. *Macromolecules* **51**, 2887–2898 (2018).

93. Cheng, Y., Yang, J., Hung, J.-H., Patra, T. K. & Simmons, D. S. Design Rules for Highly Conductive Polymeric Ionic Liquids from Molecular Dynamics Simulations. *Macromolecules* **51**, 6630–6644 (2018).

94. Plazek, D. J., Zheng, X. D. & Ngai, K. L. Viscoelastic properties of amorphous polymers. I. Different temperature dependences of segmental relaxation and terminal dispersion. *Macromolecules* **25**, 4920–4924 (1992).

95. Lang, R. J. & Simmons, D. S. Interfacial Dynamic Length Scales in the Glass Transition of a Model Freestanding Polymer Film and Their Connection to Cooperative Motion. *Macromolecules* **46**, 9818–9825 (2013).

96. Baschnagel, J. & Varnik, F. Computer simulations of supercooled polymer melts in the bulk and in confined geometry. *J. Phys. Condens. Matter* **17**, R851–R953 (2005).

97. Starr, F. W., Douglas, J. F. & Sastry, S. The relationship of dynamical heterogeneity to the Adam-Gibbs and random first-order transition theories of glass formation. *J. Chem. Phys.* **138**, 12A541-12A541-18 (2013).

98. Simmons, D. S. & Douglas, J. F. Nature and interrelations of fast dynamic properties in a coarse-grained glass-forming polymer melt. *Soft Matter* **7**, 11010–11020 (2011).

99. Hsu, D. D., Xia, W., Song, J. & Keten, S. Glass-Transition and Side-Chain Dynamics in Thin Films: Explaining Dissimilar Free

Surface Effects for Polystyrene vs Poly(methyl methacrylate). *ACS Macro Lett.* **5**, 481–486 (2016).

100. Shavit, A. & Riggleman, R. A. Influence of Backbone Rigidity on Nanoscale Confinement Effects in Model Glass-Forming Polymers. *Macromolecules* **46**, 5044–5052 (2013).

101. De Gennes, P. G. Liquid dynamics and inelastic scattering of neutrons. *Physica* **25**, 825–839 (1959).

102. Mangalara, J. H. & Simmons, D. S. Tuning Polymer Glass Formation Behavior and Mechanical Properties with Oligomeric Diluents of Varying Stiffness. *ACS Macro Lett.* **4**, 1134–1138 (2015).

103. Ruan, D. & Simmons, D. S. Roles of chain stiffness and segmental rattling in ionomer glass formation. *J. Polym. Sci. Part B Polym. Phys.* n/a-n/a (2015). doi:10.1002/polb.23788

104. Lang, R. J. & Simmons, D. S. Interfacial Dynamic Length Scales in the Glass Transition of a Model Freestanding Polymer Film and Their Connection to Cooperative Motion. *Macromolecules* **46**, 9818–9825 (2013).

105. Vogel, H. Das temperatur-abhängigkeitsgesetz der viskosität von flüssigkeiten. *Phys Zeit* **22**, 645–646 (1921).

106. Fulcher, G. S. Analysis of recent measurements of the viscosity of glasses. *J Am Ceram Soc* **8**, 339 (1925).

107. Tammann, G. & Hesse, W. Die abhängigkeit der viskosität von der temperatur bei unterkühlten flüssigkeiten. *Z Anorg Allg Chem* **156**, 245–257 (1926).

108. Schmidtke, B., Hofmann, M., Lichtinger, A. & Rössler, E. A. Temperature Dependence of the Segmental Relaxation Time of Polymers Revisited. *Macromolecules* **48**, 3005–3013 (2015).

109. Kremer, K. & Grest, G. S. Molecular dynamics (MD) simulations for polymers. *J. Phys. Condens. Matter* **2**, SA295–SA298 (1990).

110. Varnik, F., Baschnagel, J. & Binder, K. Reduction of the glass transition temperature in polymer films: A molecular-dynamics study. *Phys. Rev. E* **65**, 021507 (2002).

111. Buchholz, J., Paul, W., Varnik, F. & Binder, K. Cooling rate dependence of the glass transition temperature of polymer melts: Molecular dynamics study. *J. Chem. Phys.* **117**, 7364–7372 (2002).

112. Barrat, J.-L., Baschnagel, J. & Lyulin, A. Molecular dynamics simulations of glassy polymers. *Soft Matter* **6**, 3430–3446 (2010).

113. Ruan, D. & Simmons, D. S. Glass Formation near Covalently Grafted Interfaces: Ionomers as a Model Case. *Macromolecules* **48**, 2313–2323 (2015).

114. Lee, J., Mangalara, J. H. & Simmons, D. S. Correspondence between the rigid amorphous fraction and nanoconfinement effects on glass formation. *J. Polym. Sci. Part B Polym. Phys.* **55**, 907–918 (2017).

115. Sastry, S. The relationship between fragility, configurational entropy and the potential energy landscape of glass-forming liquids. *Nature* **409**, 164–167 (2001).

116. Jorgensen, W. L., Maxwell, D. S. & Tirado-Rives, J. Development and Testing of the OPLS All-Atom Force Field on Conformational Energetics and Properties of Organic Liquids. *J. Am. Chem. Soc.* **118**, 11225–11236 (1996).

117. Kaminski, G. A., Friesner, R. A., Tirado-Rives, J. & Jorgensen, W. L. Evaluation and Reparametrization of the OPLS-AA Force Field for Proteins via Comparison with Accurate Quantum Chemical Calculations on Peptides. *J. Phys. Chem. B* **105**, 6474–6487 (2001).

118. Ponder, J. W. & Richards, F. M. An efficient newton-like method for molecular mechanics energy minimization of large molecules. *J. Comput. Chem.* **8**, 1016–1024 (1987).

119. Kundrot, C. E., Ponder, J. W. & Richards, F. M. Algorithms for calculating excluded volume and its derivatives as a function of molecular conformation and their use in energy minimization. *J. Comput. Chem.* **12**, 402–409 (1991).

120. Siu, S. W. I., Pluhackova, K. & Böckmann, R. A. Optimization of the OPLS-AA Force Field for Long Hydrocarbons. *J. Chem. Theory Comput.* **8**, 1459–1470 (2012).

121. Rossi, G., Monticelli, L., Puisto, S. R., Vattulainen, I. & Ala-Nissila, T. Coarse-graining polymers with the MARTINI force-field: polystyrene as a benchmark case. *Soft Matter* **7**, 698 (2011).

122. Becker, C. A., Tavazza, F., Trautt, Z. T. & Buarque de Macedo, R. A. Considerations for choosing and using force fields and interatomic potentials in materials science and engineering. *Curr. Opin. Solid State Mater. Sci.* **17**, 277–283 (2013).

123. Wu, H. H. & Trinkle, D. R. Cu/Ag EAM potential optimized for heteroepitaxial diffusion from ab initio data. *Comput. Mater. Sci.* **47**, 577–583 (2009).

124. Yamahara, K., Okazaki, K. & Kawamura, K. Molecular dynamics study of the thermal behaviour of silica glass/melt and cristobalite. *J. Non-Cryst. Solids* **291**, 32–42 (2001).

125. Hanwell, M. D. *et al.* Avogadro: an advanced semantic chemical editor, visualization, and analysis platform. *J. Cheminformatics* **4**, 17 (2012).

126. Plimpton, S. Fast Parallel Algorithms for Short-Range Molecular Dynamics. *J. Comput. Phys.* **117**, 1–19 (1995).

127. Jewett, A. I., Zhuang, Z. & Shea, J.-E. Moltemplate a Coarse-Grained Model Assembly Tool. *Biophys. J.* **104**, 169a (2013).

128. Martínez, L., Andrade, R., Birgin, E. G. & Martínez, J. M. PACKMOL: A package for building initial configurations for molecular dynamics simulations. *J. Comput. Chem.* **30**, 2157–2164 (2009).

129. Tuckerman, M., Berne, B. J. & Martyna, G. J. Reversible multiple time scale molecular dynamics. *J. Chem. Phys.* **97**, 1990–2001 (1992).

130. Hopkins, C. W., Le Grand, S., Walker, R. C. & Roitberg, A. E. Long-Time-Step Molecular Dynamics through Hydrogen Mass Repartitioning. *J. Chem. Theory Comput.* **11**, 1864–1874 (2015).

131. Harmandaris, V. A. & Kremer, K. Dynamics of Polystyrene Melts through Hierarchical Multiscale Simulations. *Macromolecules* **42**, 791–802 (2009).

132. Feenstra, K. A., Hess, B. & Berendsen, H. J. C. Improving efficiency of large time-scale molecular dynamics simulations of hydrogen-rich systems. *J. Comput. Chem.* **20**, 786–798 (1999).

133. Humprey, W., Dalke, A. & Schulten, K. VMD - Visual Molecular Dynamics. *J. Mol. Graph.* **14**, 33–38 (1996).

134. Starr, F. W., Sastry, S., Douglas, J. F. & Glotzer, S. C. What do we learn from the local geometry of glass-forming liquids? *Phys. Rev. Lett.* **89**, 125501 (2002).

135. Cicerone, M. T., Zhong, Q., Johnson, J., Aamer, K. A. & Tyagi, M. Surrogate for Debye–Waller Factors from Dynamic Stokes Shifts. *J Phys Chem Lett* **2**, 1464–1468 (2011).

136. Bellissent-Funel, M. C., Filabozzi, A. & Chen, S. H. Measurement of coherent Debye-Waller factor in in vivo deuterated C-phycocyanin by inelastic neutron scattering. *Biophys. J.* **72**, 1792–1799 (1997).

137. Frauenfelder, H. *et al.* A unified model of protein dynamics. *Proc. Natl. Acad. Sci.* **106**, 5129–5134 (2009).

138. Weiss, R. J., Demarco, J. J., Weremchuk, G., Hastings, J. & Corliss, L. Anisotropic Debye-Waller Factors in Cubic Crystals. *Phys. Rev.* 1420 (1954).

139. Betancourt, B. A. P., Douglas, J. F. & Starr, F. W. String model for the dynamics of glass-forming liquids. *J. Chem. Phys.* **140**, 204509 (2014).

140. Puosi, F., Chulkin, O., Bernini, S., Capaccioli, S. & Leporini, D. Thermodynamic scaling of vibrational dynamics and relaxation. *J. Chem. Phys.* **145**, 234904 (2016).

141. Iwashita, T., Nicholson, D. M. & Egami, T. Elementary Excitations and Crossover Phenomenon in Liquids. *Phys. Rev. Lett.* **110**, 205504 (2013).

142. Blodgett, M. E., Egami, T., Nussinov, Z. & Kelton, K. F. Proposal for universality in the viscosity of metallic liquids. *Sci. Rep.* **5**, srep13837 (2015).

143. Ottochian, A. & Leporini, D. Universal scaling between structural relaxation and caged dynamics in glass-forming systems: Free volume and time scales. *J. Non-Cryst. Solids* **357**, 298–301 (2011).

144. Engberg, D. *et al.* Sound waves and other modes in the strong glass former B2O3. *Phys. Rev. B* **58**, 9087–9097 (1998).

145. Napolitano, A., Macedo, P. B. & Hawkins, E. G. Viscosity and Density of Boron Trioxide. *J. Am. Ceram. Soc.* **48**, 613–616 (1965).

146. Buchenau, U. & Zorn, R. A Relation Between Fast and Slow Motions in Glassy and Liquid Selenium. *EPL Europhys. Lett.* **18**, 523 (1992).

147. Buchenau, U., Wischnewski, A., Richter, D. & Frick, B. Is the Fast Process at the Glass Transition Mainly due to Long Wavelength Excitations? *Phys. Rev. Lett.* **77**, 4035–4038 (1996).

148. Kariyo, S. *et al.* From Simple Liquid to Polymer Melt. Glassy and Polymer Dynamics Studied by Fast Field Cycling NMR Relaxometry: Rouse Regime. *Macromolecules* **41**, 5322–5332 (2008).

149. Sastry, S., Truskett, T. M., Debenedetti, P. G., Torquato, S. & Stillinger, F. H. Free volume in the hard sphere liquid. *Mol. Phys.* **95**, 289–297 (1998).

150. White, R. P. & Lipson, J. E. G. Free Volume in the Melt and How It Correlates with Experimental Glass Transition Temperatures: Results for a Large Set of Polymers. *Acs Macro Lett.* **4**, 588–592 (2015).

151. Zhao, J., Simon, S. L. & McKenna, G. B. Using 20-million-year-old amber to test the super-Arrhenius behaviour of glass-forming systems. *Nat. Commun.* **4**, 1783 (2013).

152. Singh, S., Ediger, M. D. & Pablo, J. J. de. Ultrastable glasses from in silico vapour deposition. *Nat. Mater.* **12**, 139–144 (2013).

153. Simmons, D. S., Cicerone, M. T. & Douglas, J. F. Response to "Comment on 'Generalized Localization Model of Relaxation in Glass-Forming Liquids'" by A. Ottochian et al. *Soft Matter* **9**, 7892–7899 (2013).

154. Plazanet, M. & Schober, H. Anharmonicity in a fragile glass-former probed by inelastic neutron scattering. *Phys. Chem. Chem. Phys.* **10**, 5723–5729 (2008).

155. Forrey, C. *et al.* Prediction and validation of diffusion coefficients in a model drug delivery system using microsecond atomistic molecular dynamics simulation and vapour sorption analysis. *Soft Matter* **10**, 7480–7494 (2014).

156. Mirigian, S. & Schweizer, K. S. Communication: Slow relaxation, spatial mobility gradients, and vitrification in confined films. *J. Chem. Phys.* **141**, 161103 (2014).

157. Mirigian, S. & Schweizer, K. S. Elastically cooperative activated barrier hopping theory of relaxation in viscous fluids. II. Thermal liquids. *J. Chem. Phys.* **140**, 194507 (2014).

158. Vogel, H. Das temperatur-abhängigkeitsgesetz der viskosität von flüssigkeiten. *Phys Zeit* **22**, 645–646 (1921).

159. Fulcher, G. S. Analysis of recent measurements of the viscosity of glasses. *J Am Ceram Soc* **8**, 339 (1925).

160. Phan, A. D. & Schweizer, K. S. Elastically Collective Nonlinear Langevin Equation Theory of Glass-Forming Liquids: Transient Localization, Thermodynamic Mapping, and Cooperativity. *J. Phys. Chem. B* (2018). doi:10.1021/acs.jpcb.8b04975

‡ This figure is based upon a small sampling of simulation studies of dynamics in supercooled liquids over the last 30 years. We limit this survey to studies using purely molecular dynamics simulations (i.e. no Monte Carlo or accelerated dynamics methods). For each study, we extracted the largest reported relaxation time of the entire simulated system. Where a relaxation time was not directly reported, we estimated a relaxation time from relaxation function curves. We required that the relaxation time be directly simulated and not extrapolated from fits to shorter-time data, and we attempted to exclude studies with abbreviated or ill-defined annealing protocols that left the state of equilibration uncertain.

Table of contents graphic

High-throughput simulations reveal a universal onset of particle localization in diverse glass-forming liquids.